

Machine learning modeling of family wide enzyme-substrate specificity screens

Samuel Goldman,^{†,‡} Ria Das,^{‡,¶} Kevin K. Yang,[§] and Connor W. Coley^{*,‡,¶}

[†]*MIT Computational and Systems Biology*

[‡]*MIT Chemical Engineering*

[¶]*MIT Electrical Engineering and Computer Science*

[§]*Microsoft Research New England*

E-mail: ccoley@mit.edu

Abstract

Biocatalysis is a promising approach to sustainably synthesize pharmaceuticals, complex natural products, and commodity chemicals at scale. However, the adoption of biocatalysis is limited by our ability to select enzymes that will catalyze their natural chemical transformation on non-natural substrates. While machine learning and *in silico* directed evolution are well-posed for this predictive modeling challenge, efforts to date have primarily aimed to increase activity against a single known substrate, rather than to identify enzymes capable of acting on new substrates of interest. To address this need, we curate 6 different high-quality enzyme family screens from the literature that each measure multiple enzymes against multiple substrates. We compare machine learning-based compound-protein interaction (CPI) modeling approaches from the literature used for predicting drug-target interactions. Surprisingly, comparing these interaction-based models against collections of independent (single task) enzyme-only or substrate-only models reveals that current CPI approaches are incapable of learning interactions between compounds and proteins in the current family level data regime.

We further validate this observation by demonstrating that our no-interaction baseline can outperform CPI-based models from the literature used to guide the discovery of kinase inhibitors. Given the high performance of non-interaction based models, we introduce a new structure-based strategy for pooling residue representations across a protein sequence. Altogether, this work motivates a principled path forward in order to build and evaluate meaningful predictive models for biocatalysis and other drug discovery applications.

Introduction

Biology has evolved enzymes that are capable of impressively stereo-selective, regio-selective, and sustainable chemistry to produce compounds and perform reactions that are “the envy of chemists”.¹⁻³ Industrial integration of these enzymes in catalytic processes is transforming our bioeconomy, with engineered enzymes now producing various materials and medicines on the market today.^{2,4} As an exemplar of collective progress in biocatalysis and enzyme engineering, Huffman et al. impressively re-purposed the entire nucleoside salvage pathway for a high yield, 9-enzyme *in vitro* synthesis of the HIV nucleoside analogue drug, islatravir.⁵ In an effort to make these types of pathways commonplace, there has been an explosion in new tools for automated computer-aided synthesis planning (CASP) that can include not only traditional organic chemistry reactions,⁶ but also enzymatic reactions, facilitating further growth of industrial biocatalysis.⁷⁻⁹

Despite this progress in synthesis planning, suggesting an enzyme for each catalytic step in a proposed synthesis pathway remains difficult and limits the practical utility of synthesis planning software. Current enzyme selection methods often use simple similarity searches, comparing the desired reaction to precedent reactions in a database.¹⁰ Due to the often high selectivity of enzymes, proposed enzymes for a hypothetical reaction step often suffer from low catalytic efficiency. In the extreme case, the proposed enzyme may have zero catalytic effect on the substrate of interest, despite showing moderate activity on a similar natural

substrate. Thus, the specificity of enzymatic catalysis can be a double edged sword.¹¹ As an example, the phosphorylation step in the islatravir synthesis of Huffman et al. required screening a multitude of natural kinase classes to find an enzyme capable of phosphorylating the desired substrate with sufficient activity for subsequent directed evolution.⁵ In the less extreme case, the enzyme of interest may have moderate activity but suffer from low initial substrate loadings, proceed slowly, require higher catalyst loadings, and produce low yields.² Nevertheless, an enzyme with moderate activity can serve as a “hook” for further experimental optimization and directed evolution efforts.

Machine learning and predictive modeling provide an avenue to accelerate long development cycles and identify enzymes with both initial activity and high efficiency. Sequence-based machine learning methods have already been utilized in “machine learning guided directed evolution” (MLDE) campaigns to help guide the exploration of sequence space toward desirable protein sequences.^{12–14} MLDE demonstrations often follow a similar paradigm: given a screen of a single enzyme with mutations at select positions, predict the function or activity of enzymes with new mutations. Further developments in pretrained machine learning models can now provide meaningful embeddings at single amino acid positions that capture contextual and structural information about the protein from sequence alone.^{15–19} These pre-trained embeddings have proved especially useful for the application of MLDE in low-N settings where the number of protein measurements is small (Fig. 1A).^{20,21} Altogether, these approaches provide a way to improve the efficiency of an enzyme given examples of other enzymes with activity on the substrate of interest. However, this paradigm does not extend to meet the the challenge of identifying a “hook” enzyme with sufficient initial activity on a non-native substrate, nor can current approaches incorporate information from enzymes measured on *other* substrates.

Instead, work to date to expand the substrate scope of an enzyme class of interest often relies upon time consuming and *ad hoc* rational engineering based upon structure,^{22,23} simple similarity searches between the native substrate and desired substrate of interest,²⁴ or

trial-and-error experimental sampling.²⁵ Once an enzyme with some activity for a substrate of interest is found practitioners can resume directed evolution strategies similar to those described above to increase efficiency.²⁵⁻²⁸

The last strategy of experimental sampling often involves broad metagenomic sampling,²⁹⁻³¹ where homologous sequences are chosen for testing.³¹⁻³³ Researchers will test a diverse set of “mined” enzymes for activity against a panel of substrates containing the relevant reactive group. This experimental screening of enzymes against substrates closely mirrors the data setting involved in discovering selective inhibitors in drug discovery, where a panel of similar proteins such as kinases³⁴ or deubiquinating proteins^{35,36} are screened against a family of compounds. While some work in this field of compound protein interactions (CPI) has attempted to model the drug discovery framing of this problem,^{37,38} the CPI modeling framework has not yet been extended to enzyme promiscuity and there exist few curated datasets to probe our ability to learn from enzyme screens.

In this work, we model enzyme-substrate compatibility as a compound-protein interaction task using a carefully curated set of recent metagenomic enzyme family screens from the literature. We compare state of the art predictive modeling using pretrained embedding strategies (for both small molecules and proteins) and CPI prediction models. Surprisingly, we find that predictive models trained jointly on enzymes and substrates fail to outperform independent, single-task enzyme-only or substrate-only models, indicating that the joint models are incapable of learning interactions. To determine whether this is a quirk specific to our datasets, we reanalyze a recent CPI demonstration and find that this trend generalizes beyond enzyme-substrate data to CPI more broadly: learning interactions from protein family data to go beyond single-task models remains an open problem. Finally, we introduce a new pooling strategy specific to metagenomically-sampled enzymes using a multiple sequence alignment (MSA) and reference crystal structure to enhance enzyme embeddings and improve model performance on the task of enzyme activity prediction. Collectively, this work lays the foundation and establishes dataset standards for the construction of robust

enzyme-substrate compatibility models that are needed for various downstream applications such as biosynthesis planning tools.

Results

Data summary

In order to systematically evaluate our ability to build models over enzyme-substrate interactions, we first need high quality data. Databases of metabolic reactions such as BRENDA³⁹ describe large numbers of known enzymatic reactions, but are collected from many sources at different concentrations, temperatures, and pH values. Instead, we turn to the literature to find high-throughput enzymatic activity screens with standardized procedures, i.e., exhibiting no variation in the experiments besides the identities of the small molecule and enzyme. We extract amino acid sequences and substrate SMILES strings from six separate studies measuring the activity of halogenase,⁴⁰ glycosyltransferase,⁴¹ thiolase,⁴² β -keto acid cleavage enzymes (BKACE),⁴³ esterase,⁴⁴ and phosphatase enzymes⁴⁵ which cover between 1,000 and 36,000 enzyme-substrate pairs (Tab. 1). Enzymatic catalysis (e.g., yield, conversion, activity) in each study was measured using some combination of coupled assay reporters, mass spectrometry, or fluorescent substrate readouts. Data was binarized such that every measured pair is either labeled as active (1) or inactive (0) at thresholds according to standards described in the original papers (Methods). We conceptualize these datasets as “dense screens” insofar as each dataset represents a number of enzyme and substrate pairs measured against each other resembling a grid (Fig. 1B). While several of the experimental papers presenting these datasets include their own predictive modeling,^{41–43} these demonstrations are not systematically compared with standard splits and are not easily evaluated against new methods due to varied data formats. In compiling these, we expose new datasets to the protein machine learning community. Additional details can be found in the Methods.

In order to evaluate the ability of data-driven models to generalize beyond the set of

screened enzymes and substrates, we examine extrapolation in two directions: enzyme discovery or substrate discovery (Fig. 1C). In the former, we consider the setting of a practitioner who is interested in finding enzymes with activity on some set of substrates they’ve already measured. This parallels the setting where machine learning directed evolution may also be applied, such as increasing the efficiency of an enzyme (Fig. 1A). On the other hand, for substrate discovery, we are interested in predicting which enzymes from an already-sampled set will act on a new substrate that has not already been measured, a formulation specifically relevant to synthesis planning. We omit the more difficult problem of generalizing to new substrates and new enzymes simultaneously; we posit that we must first be able to generalize in each direction separately in order to generalize jointly. We do not consider the task of interpolation within a dense screen (Fig. 1B), as this does not reflect any realistic experimental application.

Models

We aim to build a modeling pipeline that accepts both an enzyme and substrate and predicts sequence, with enzymes and substrates specified by sequence and SMILES strings respectively. To featurize enzymes, we turn to pre-trained protein language models, specifically the currently state-of-the-art ESM-1b model.¹⁸ Pre-trained representations are well-suited to low data tasks and have been applied to protein property prediction^{18–20} as well as compound protein interaction.⁴⁶ To featurize substrates, we test an analogously pretrained Junction-Tree Variational Auto-Encoder (JT-VAE),⁴⁷ following a recent CPI approach,³⁷ as well as traditional, 1024 bit Morgan circular fingerprints.⁴⁸

If a single model is able to successfully learn interactions and leverage the full “dense” dataset, it should be able to take as input both enzyme and substrate representations and outperform smaller, single-task models that either use only enzyme inputs or use only substrate inputs (Fig. 1C). To attempt to model interactions, we consider two simple top models inspired by the CPI literature^{37,38,46} that either (1) concatenate the representations of the

enzyme and substrate before applying a shallow feed forward neural network or (2) project the representations of the enzyme and substrate to smaller and equal length vectors before taking their dot product (Fig. 1D).

Table 1: Summary of curated datasets with the number of unique enzymes, unique substrates, and unique pairs in each dataset in addition to an exemplar structure for the protein family.

Dataset	# Enz.	# Sub.	Pairs	PDB Ref.
Halogenase ⁴⁰	42	62	2,604	2AR8
Glycosyltransferase ⁴¹	54	90	4,298 ^a	3HBF
Thiolase ⁴²	73	15	1,095	4KU5
BKACE ⁴³	161	17	2,737	2Y7F
Phosphatase ⁴⁵	218	165	35,970	3L8E
Esterase ⁴⁴	146	96	14,016	5A6V
Kinase (inhibitors) ³⁴	318	72	22,896	2CN5

^a While most datasets we use test all combinations, Yang et al. do not report experiments for some enzyme by substrate interactions

Enzyme discovery

We test these various featurizations and model architectures first on the task of enzyme discovery. To do so, we hold out a fraction of the enzymes as a test set and use the training set to make predictions about the interactions between the held out enzymes and the known substrates in the data set. We train the CPI model architectures described above jointly on the entire training set. To test whether CPI models are able to learn interactions, we also train several smaller “single-task” models. These single-task models are specific to each substrate and accept only an enzyme sequence as input. If models are in fact able to learn interactions, the CPI models should outperform the single-task models given their access to more substrate measurements for each enzyme (Fig. 2A, 1C).

To evaluate each dataset, we calculate the area under the precision recall curve (AUPRC), computed separately for each substrate column and subsequently averaged. AUPRC is able to better differentiate model performance on highly imbalanced data than the area under the receiver operating curve (AUROC), which overvalues the prediction of true negatives.

Further, AUPRC does not require choosing a threshold to call hits like other metrics like the Matthews Correlation Coefficient. We optimize model hyperparameters on the thiolase dataset⁴² prior to training and evaluating on the remaining five datasets.

We observe that our supervised models using pretrained protein representations are in fact able to outperform a nearest neighbor sequence-similarity baseline (“KNN: Levenshtein”) that uses the Levenshtein distance to predict held out enzyme activity (Fig. 2B, Tab. S3,S4). This affirms the potential of representation learning to improve prediction and protein engineering tasks.

Surprisingly, however, CPI models do not outperform single-task models trained with simple logistic regression (“Ridge: ESM-1b”) (Fig. 2B). This is despite the CPI models having access to a larger number of enzyme-substrate interactions for training. In fact, models trained with CPI can at times perform worse than models that predict the activity of enzymes on each substrate task independently (Fig. 2C), indicating an inability to learn interactions from the dense screens collected.

The enzymes within each dataset were sampled with different levels of diversity by the studies’ original authors. The phosphatase dataset represents a diverse super-family of enzymes,⁴⁵ whereas the BKACE dataset represents a more narrowly sampled domain of unknown function (unknown prior to the experimental screen).⁴³ We find that the average pairwise Levenshtein similarity between sequences in the dataset is in fact correlated with performance differences across datasets, such that more similar datasets seem to be easier to predict (Fig. 2D).

In addition to intra-dataset diversity, we also hypothesized that the balance, or fraction of active enzymes, observed for each enzyme could partially explain the observed performance. Plotting the number of active enzymes against each substrate in the datasets reveals a strong positive correlation, validating that the number of hits observed in the training set will largely determine the success of the model in generalizing beyond the training set. This is equally a function of both the models and the AUPRC metric, which follows a similar trend for

random guesses that favor the majority binary class.

Substrate discovery

We next evaluate generalization in the direction of held out substrates, repeating the same procedures as above. In this case, we restrict our analysis only to the glycosyltransferase and phosphatase datasets where the number of substrates is > 50 , using the halogenase dataset to tune hyperparameters for each model. Similar to our conclusions in the case of enzyme discovery, we find that the CPI architectures are not able to outperform simpler, single-task logistic regression models with Morgan fingerprints (Fig. 3, S5; Tab. S5, S6).

Curiously, in both the enzyme discovery (Fig. S9 S10, S8, S7, S11) and substrate discovery (Fig. S13, S12, S14) settings, predictions made by CPI models exhibit far more “blocky” characteristics than the respective single task models: when extrapolating to new enzymes, the prediction variance is not sensitive to the paired substrate for CPI models. This indicates that our CPI models struggle to condition their predictions to new enzymes (substrates) based upon the substrate (enzyme) pairing.

Reanalysis of kinase inhibitor discovery

The results for enzyme-substrate activity prediction demonstrate that models designed to learn interactions are seemingly unable to do so in a manner that improves generalization. We therefore wondered to what extent this failing was specific to enzyme-substrate data, as opposed to being symptomatic of a broader problem and shortcoming in the CPI field, including drug discovery. To interrogate this, we re-analyze models from a recent study leveraging an inhibitor screen against the human kinome to discover new inhibitors against tuberculosis.³⁷ In their study, Hie et al. train CPI models on a dense screen of 442 kinases against 72 inhibitors³⁴ using concatenated pretrained protein and pretrained substrate features as the input to multi layer perceptrons (MLP), Gaussian processes (GPs), or a combination of the two (GP + MLP), the combination being their most successful (Methods).

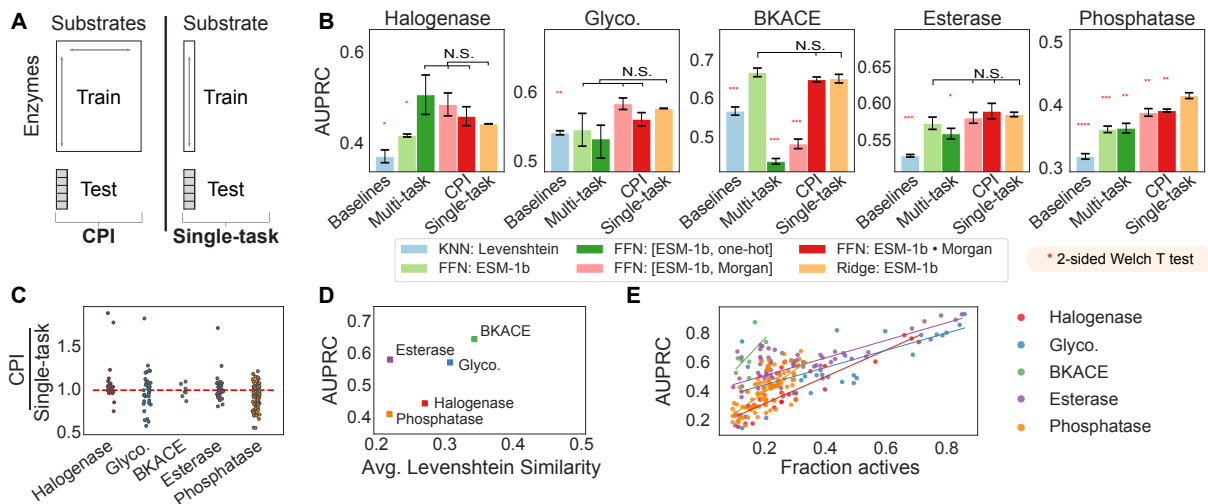


Figure 2: Assessing enzyme discovery in family wide screens. (A) CPI models are compared against the single task setting by holding out enzymes for a given substrate and allowing models to train on either the full expanded data (CPI) or only data specific to that substrate (single-task). (B) AUPRC is compared on five different datasets, arranged from left to right in order of increasing number of enzymes in the dataset. K-nearest-neighbor (KNN) baselines with Levenshtein edit distance are compared against feed forward networks (FFN) and ridge regression models. Two compound protein interaction architectures are tested, both concatenation and dot-product, indicated with “[{prot repr.}, {sub repr.}]” and “[{prot repr.}•{sub repr.}]” respectively. ESM-1b features indicate protein features extracted from a masked language model trained on UniRef50.¹⁸ Multi-task models indicate models in which a single model jointly predicts all enzyme-substrate activities with a shared intermediate, but no explicit representation of the compound is included. Halogenase and glycosyltransferase datasets are evaluated using leave-one-out splits, whereas BKACE, phosphatase, and esterase datasets are evaluated with 5 repeats of 10 different cross validation splits. Standard error bars indicate the standard error of the mean of results computed with 3 random seeds. Each method is compared to an L2-regularized logistic regression model (“Ridge: ESM-1b”) using a 2-sided Welch T test, with each additional asterisk representing significance at [0.05, 0.01, 0.001, 0.0001] thresholds respectively after application of a Benjamini-Hochberg correction. (C) Average AUPRC on each individual “substrate task” is compared between compound protein interaction models and single-task models. Points below 1 indicate substrates on which single-task models better predict enzyme activity than CPI models. CPI models used are FFN: [ESM-1b, Morgan] and single-task models are Ridge: ESM-1b. (D) AUPRC values from the ridge regression model are plotted against the average enzyme similarity in a dataset, with higher enzyme similarity revealing better predictive performance. (E) AUPRC values from the ridge regression model broken out by each task are plotted against the fraction of active enzymes in the dataset. Best fit lines are drawn through each dataset to serve as a visual guide.

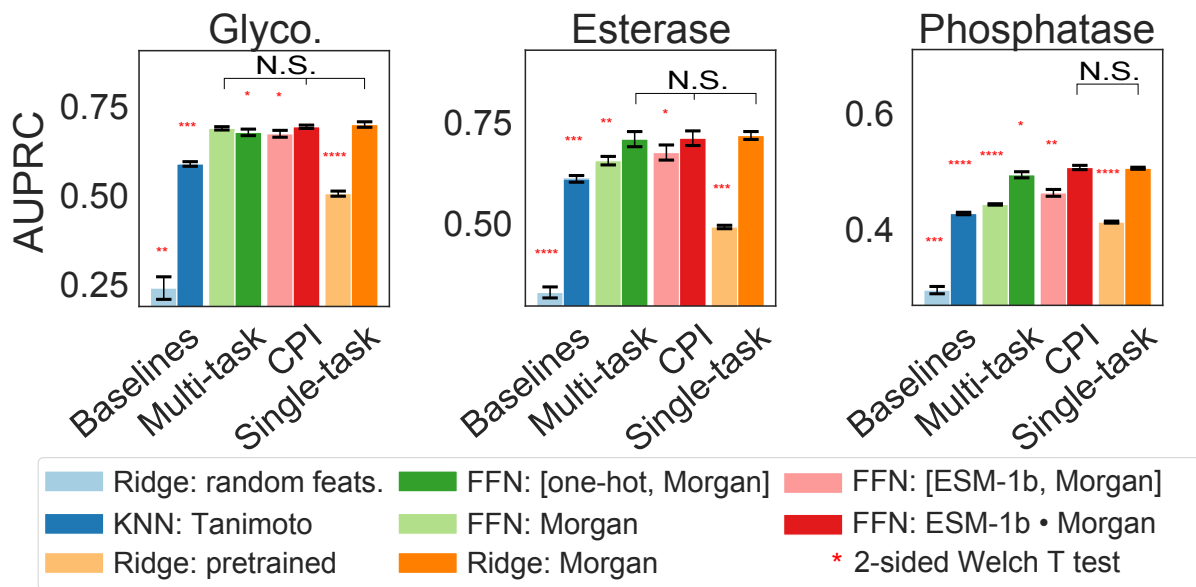


Figure 3: **Assessing substrate discovery in family wide screens.** CPI models and single task models are compared on the glycosyltransferase, esterase, and phosphatase datasets, all with 5 trials of 10-fold cross validation. Error bars represent the standard error of the mean across 3 random seeds. Each model and featurization is compared to “Ridge: Morgan” using a 2-sided Welch T test, with each additional asterisk representing significance at [0.05, 0.01, 0.001, 0.0001] thresholds respectively, after applying a Benjamini-Hochberg correction. Pretrained substrate featurizations used in “Ridge: pretrained” are features extracted from a junction-tree variational auto-encoder (JT-VAE).⁴⁷ Two compound protein interaction architectures are tested, both concatenation and dot-product, indicated with “[{prot repr.}, {sub repr.}]” and “[{prot repr.}•{sub repr.}]” respectively. In the interaction based architectures, ESM-1b indicates the use of a masked language model trained on UniRef50 as a protein representation.¹⁸ Models are hyperparameter optimized on a held out halogenase dataset. AUCROC results can be found in Fig. S4.

Unlike the binary classification enzyme activity setting, they predict continuous K_d values.

We compare the MLP and GP+MLP models using pretrained representations against a number of single-task models on two settings matching the original study: drug repurposing and drug discovery. Drug repurposing is analogous to enzyme discovery where certain proteins are held out; drug discovery is analogous to substrate discovery where certain compounds are held out. Single-task models are not presented with training data on other kinase-compound pairs and are therefore unable to learn interactions in a generalizable manner. In addition to the single-task MLP and GP+MLP models, we evaluate a simple single-task, L2-regularized linear regression model (“Ridge”) using Morgan fingerprint features rather than JT-VAE features. In concordance with our results on enzymatic data, we find that single-task models consistently outperform CPI based models in terms of Spearman correlation coefficient between true and predicted K_d on both repurposing (Fig. 4A) and discovery tasks (Fig. 4B). This shows that ablating interactions by training single-task models can increase performance over GP+MLP models.

Still, increased rank correlation between predictions and true K_d values does not necessarily equate to the ability to select new inhibitors or new drugs. To directly test this, we repeat the retrospective kinase-inhibitor lead prioritization experiments conducted in the original analysis. Models are trained on a set of kinase-inhibitor pairings and used to rank new kinase-inhibitor pairings. The acquisition preference is informed by predictions and, if applicable, predicted uncertainty (Methods). When acquiring either 5 or 25 new data points in cross validation, a single-task ridge regression model with equivalent pretrained features is able to outperform both CPI based models (Fig. 4C,D). Our findings are retrospective in nature and do not negate the value of prospective experimental validation,³⁷ but rather make clear that the field requires new methods to leverage the rich information contained in protein, small molecule interaction screens and truly learn interactions.

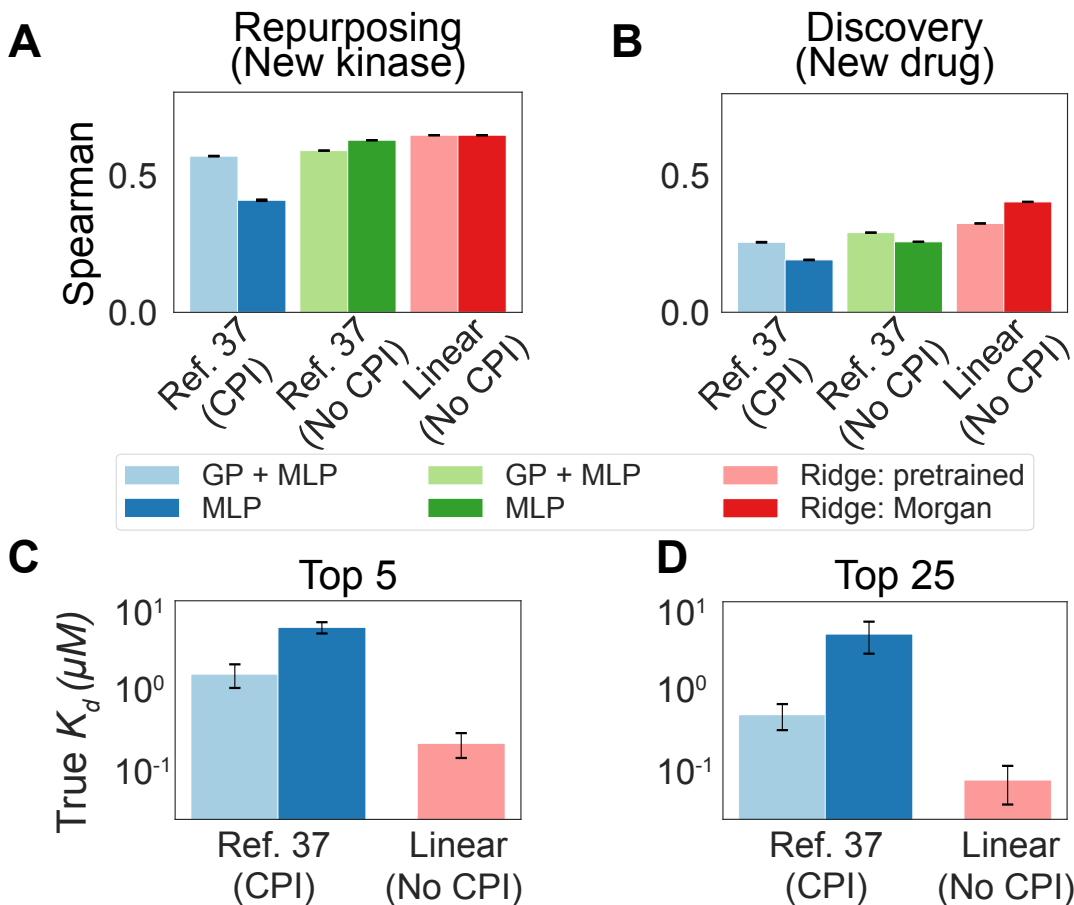


Figure 4: **Evaluating single-task models on kinase repurposing and discovery tasks** Kinase data from Davis et al. is extracted, featurized, and split as prepared in Hie et al. Multilayer perceptrons (MLP) and Gaussian process + multilayer perceptron (GP+MLP) models are employed. We add variants of these models without CPI training separate single-task models for each enzyme and substrate in the training set, as well as linear models using both pretrained featurizations (“Ridge: pretrained”) and fingerprint based featurizations of small molecules (“Ridge: Morgan”). Spearman correlation is shown for **(A)** held out kinases not in the training set and **(B)** held out small molecules not in the training set across 5 random initializations. **(C)** We repeat the retrospective evaluation of lead prioritization. The top 5 average acquired K_d values are shown for the CPI models in Hie et al. compared against a linear, single-task ridge regression model using the same features. **(D)** The top 25 average acquired K_d values are shown.

Improving enzyme discovery models

Given that single-task models appear to match or even outperform models design for CPI, we next asked if we could improve their generalization in the enzyme discovery direction by leveraging the relationship between different protein sequences within the dataset. That is, working within a single family of proteins *should* be more conducive to generalizations. To directly impart this structural bias on our models, we considered how the construction of the pretrained representation for each protein could be modified. Pretrained language models produce a fixed dimensional embedding at each amino acid position in the protein. To collapse this into a fixed-length protein-level embedding, the *de facto* standard is to compute the mean embedding across the length of the sequence.^{15,18–20} However, for locally-defined properties, such as enzymatic catalysis or ligand binding at an active site, this mean pooling strategy may be sub-optimal. Previous approaches have largely considered deep mutational scans with few mutations at carefully selected positions.¹³ In these settings, mean pooling strategies may be a good approximation of local protein structural changes, as embeddings at distal positions from the mutation would be nearly constant across protein variants. In our setting, however, we have metagenomically sampled sequences with large insertions and deletions, which presents an ideal testing ground to evaluate pooling strategies.

We test 3 alternative pooling strategies to mean pooling, where we first compute a multiple sequence alignment (MSA) and pool only a subset of residues in each sequence corresponding to a subset of columns in the MSA (Fig. 5A). We rank order the columns in the MSA to be pooled based upon the (i) proximity to the active site of a single “reference structure” (ii) coverage (i.e., pooling columns with the fewest gaps), or (iii) conservation (i.e., pooling columns that have the highest frequency of any single amino acid type) (Tab. 1). To expand this analysis beyond catalysis to drug discovery, we also consider a portion of the kinase inhibitor dataset from Davis et al.,³⁴ subsetting down to a single kinase family (PF00069), rather than the whole human kinome (Tab. 1). We compare these pooling strategies across the enzyme discovery datasets tested, as well as the protein-inhibitor kinase

dataset. We use ridge regression models with pretrained ESM-1b¹⁸ embeddings, and split the data as in the enzyme discovery setting, varying only the pooling strategy from our previous analysis (Fig. 2). In the case of the kinase regression dataset, we use the Spearman rank correlation to evaluate performance.

In all cases tested, the active site pooling performance peaks when pooling only a small number of residues around the active site (< 60 amino acids), showing gains in performance over other pooling strategies as well as the mean pooling baseline (Fig. 5B). This corresponds to a distance of < 10 angstroms away from the active site (Fig. 5Ai). This may indicate an optimal range at which residue positioning is relevant to promiscuity. In the case of the kinases, the Levenshtein distance baseline outperforms the mean pooling method with respect to Spearman rank correlation, but using active site aware pooling outperforms both. Interestingly, for the halogenase dataset, no alternative pooling strategies outperform mean pooling (Fig. S6), likely because the halogenase enzymes have high variance in solubility, a global property that could be driving enzyme activity.⁴⁰ Similarly, for the esterase dataset, coverage pooling is far more effective, indicating that a combination of targeted pooling residue strategies may be most effective (Fig. S6). While performance gains from active site aware pooling are modest, this strategy provides a simple but principled way to incorporate a structural prior into enzyme prediction models, particularly for metagenomic data with high numbers of sequence indels which may introduce unwanted variance into a mean pooled protein representation.

Conclusion

Data-driven models of enzyme-substrate compatibility have the potential to drive new insights in basic biology research and also to accelerate engineering efforts focused on the design of new enzymatic synthesis routes. In addition, the same classes of models can be used for compound-protein interaction prediction for both drug discovery and drug repur-

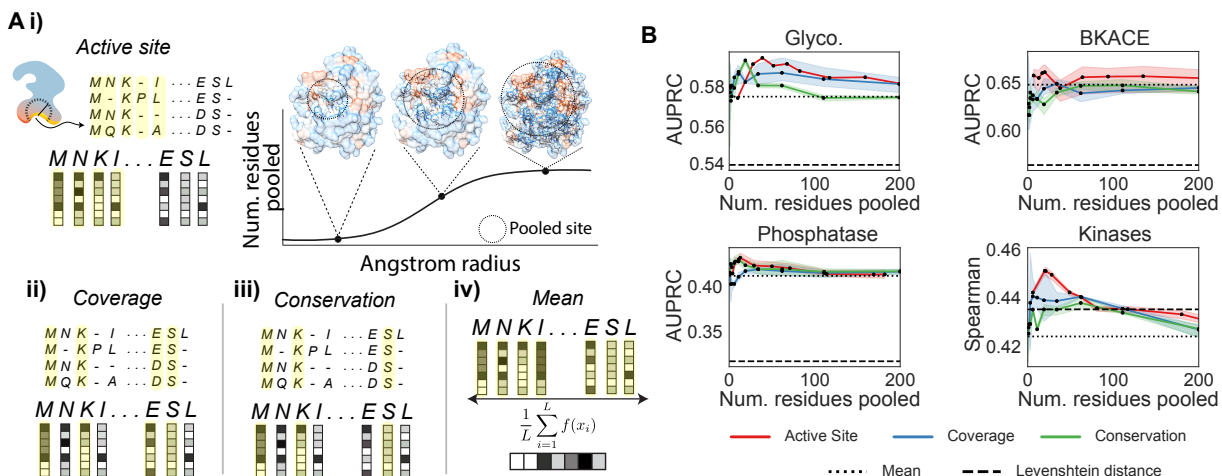


Figure 5: Structure-based pooling improves enzyme activity predictions. (A) Different pooling strategies can be used to combine amino acid representations from a pretrained protein language model. Yellow coloring in the schematic indicates residues that will be averaged to derive a representation of the protein of interest. (i) We introduce active site pooling, where only embeddings corresponding to residues within a set radius of the protein active site are averaged. By increasing the angstrom radius from the active site, we increase the number of residues pooled. Crystal structures shown are taken from the BKACE reference structure, PDB: 2Y7F rendered with Chimera.⁴⁹ (ii, iii) We also introduce two other alignment based pooling strategies: coverage and conservation pooling average only the top- k alignment columns with the fewest gaps and highest number of conserved residues respectively. (iv) Current protein embeddings often take a mean pooling strategy to indiscriminately average over all sequence positions. (B) AUPRC values are computed for various different pooling strategies are shown. Each strategy is tested for different thresholds of residues to pool, comparing against both KNN Levenshtein distance baselines and a mean pooling baseline. The same hyperparameters are used as set in Figure 2 for ridge regression models. All experiments and are repeated for 3 random seeds.

posing efforts.

In this work, we take a critical step toward opening up this suite of problems to machine learning researchers by providing several high quality, curated datasets and standardized splits to evaluate model performance and generalizability. While the small number of unique enzymes and unique substrates in each dataset makes quantitative performance sensitive to hyperparameters and dataset splitting decisions, this collection of data is an essential starting point to develop new modeling strategies and motivate future, higher throughput enzyme activity screening.

Our experiments show that pretrained representations for proteins, coupled with structure-informed pooling techniques, can go beyond standard sequence similarity based approaches to predict protein function, an exciting demonstration of how representation machine learning can impact protein engineering. Nevertheless, despite this excitement, our analysis makes clear that current CPI modeling strategies cannot consistently leverage information from multiple substrate measurements effectively, a problem broadly applicable to CPI models. That is, models designed to learn interactions do not outperform single-task models.

To predict enzyme-substrate compatibility or design selective inhibitors against a protein family, we need new strategies to jointly embed proteins and compounds to enable more robust extrapolation to new combinations thereof. Such a scheme would allow learned interactions to be more explicitly transferred from larger databases onto smaller, but higher quality screen. This will be an exciting frontier in protein and compound representation learning, as the field seeks to go beyond protein structural prediction to protein function prediction. Further, with the exception of our structure informed (MSA-informed) pooling, our analysis remains sequence based. The relative performance of structure-based tools such as molecular dynamics for the prediction of enzyme-substrate scope remains an exciting question that this data, coupled with recent advances in protein structure prediction,⁵⁰⁻⁵² can help to address.

Methods

Dataset Preparation

Each dataset is collected from their respective papers.^{34,40–45} Activity binarizations are chosen to closely mirror the original dataset preparation. Additionally, certain enzymes were filtered based upon low solubility or activity that may result from screening decisions. Further details are given in the Supplementary Information.

Davis kinase filtering

Kinases used in reanalysis of Hie et al. are tested exactly as prepared.³⁷ To evaluate structure based pooling using this dataset, we further subset the original dataset such that each entry only contains one domain from the PFAM family, PF00069, described in the SI with dataset statistics in Table 1.

Hyperparameter optimization

All hyperparameters are set on a held out enzyme-substrate dataset using the hyperparameter optimization framework Optuna.⁵³ Hyperparameter optimization is set using up to 10 trials of cross leave-one-out cross validation on the thiolase dataset and halogenase dataset for enzyme discovery and substrate discovery tasks, respectively. Hyperparameters are chosen to maximize the average area under the precision recall curve. For nearest neighbor models, the number of neighbors is treated as a hyperparameter between 1 and 10.

For logistic ridge regression models, the regularization coefficient, α is set from $\{1e-3, 1e-2, 1e-1, 1e0, 1e1, 1e2, 1e3, 1e4\}$. For both feed-forward dot product and concatenation models, hyperparameters for dropout $([0, 0.2])$, weight decay $([0, 0.01])$, hidden dimension $([10, 90])$, layers $([1, 2])$, and learning rate $([1e-5, 1e-3])$ are chosen. All neural network models are trained for 100 epochs using the Adam optimizer and Pytorch.⁵⁴

For linear ridge regression used in reanalysis of kinase data, a default hyperparameter regularizer value of $\alpha = 1e1$ is set.

Evaluation metrics

To evaluate models in the enzyme discovery direction, activity on each substrate is considered to be its own “task”. The data is divided up into a set number of folds, and models are re-trained to make predictions on each held out fold. A single, separate AUPRC value is computed for the activity on each substrate task and then averaged across substrate tasks. AUPRC values are computed using the average precision function from `sklearn`.⁵⁵ For the halogenase, thiolase, and glycosyltransferase datasets, this is done with leave-one-out cross validation. For the phosphatase, BKACE, and kinase datasets, to limit the number of trials, we use 10 fold cross validation repeated 5 times. This procedure is repeated for 3 random seeds.

An identical procedure is conducted on the task of substrate discovery, where each enzyme is separately evaluated as its own “task”. In this case, the glycosyltransferase, esterase, and phosphatase datasets are evaluated with 5 repetitions of 10 fold cross validation.

Filtering imbalanced tasks

Certain enzymes have activity on only a few substrates and certain substrates have activity on only a few enzymes. To avoid computing AUPRC values on these tasks, we filter to only incorporate tasks with a maximum fraction of either 0.9 positives or negatives. The remaining tasks can be found in Table S2.

Kinase inhibitor reanalysis

We modify the code from Hie et al. directly to reproduce their GP, GP + MLP models, and add our no-interaction models. GP + MLP models involve first fitting an MLP model

followed by a GP to predict residual loss. First, all kinases are converted into features using a pretrained language model¹⁵ and all inhibitors are converted into features using a pretrained JT-VAE⁴⁷ or Morgan fingerprints. We create a training set of kinase, inhibitor pairs with labeled K_d values, and establish 3 separate segments of the test data: new kinases (repurposing), new inhibitors (discovery), and new kinase+inhibitor pairs. The data is split into four quadrants and one quadrant is used for training models. GP and linear models are implemented with `scikit-learn`⁵⁵ and MLP models are implemented with `Keras`,⁵⁶ following parameter choices from the original study.³⁷ Linear regression models are parametrized with $\alpha = 10$ and normalization set to True. Prior to training single-task models, we standardize the regression target values based upon the training set to have a mean of 0 and variance of 1, as we find it helps with stability with less training data.

To test the ability of models to prioritize candidates, we repeat the train/test split and rank the entire test set by predicted K_d , using an additional upper confidence bound ($\beta = 1$) metric to adjust rank for the GP + MLP model that uses uncertainty. The top $k = 5$ and $k = 25$ compound-kinase pairs are evaluated by their average true K_d . All kinase-inhibitor reanalysis experiments were repeated for five random seeds.

Pooling strategies

We use the program `Muscle` with default parameters to compute a multiple sequence alignment (MSA) on each dataset for pooling. Because many positions in certain datasets have high coverage, ties are randomly broken when choosing a priority for pooling residue embeddings. This explains the large variance in the glycosyltransferase results shown (Fig. 5) taken over several seeds. Coverage and conservation based pooling strategies are sampled for $i \in \{1, 2, 3, 6, 11, 19, 34, 62, 111, 200\}$ pooling residues, each repeated for 3 random seeds.

Active site pooling

To pool over active sites of proteins, we identify a reference crystal structure within each protein family or super family (Tab. 1). For each of these crystal structures, we select either an active site bound ligand or active site residue from the literature. We attempt to pool residues within a Cartesian distance from these sites ranging from 3 to 30 angstroms to roughly mirror the number of residues pooled for coverage and conservation methods. Angstrom shells are calculated using Biopython⁵⁷ and an in depth list of active sites used can be found in Table S1.

Code and Data Availability

All code and enzyme data can be found on GitHub at <https://github.com/samgoldman97/enzyme-datasets>. Code to reproduce models can be found at <https://github.com/samgoldman97/enz-pred>. Code to reproduce the reanalysis on the kinase data from Davis et al. can be found at <https://github.com/samgoldman97/kinase-cpi-reanalysis>.

Acknowledgement

The authors thank Brian Hie, Bryan Bryson, and Bonnie Berger for discussion around kinase inhibitor screening. The authors thank Karine Bastard, Marcel Salanoubat, Ben Davis, and Charlie Fehl for helpful discussions around their respective experimental screens. The authors acknowledge the MIT SuperCloud and Lincoln Laboratory Supercomputing Center for providing HPC resources and the MIT Machine Learning for Pharmaceutical Discovery and Synthesis consortium for partially funding this work.

References

- (1) Lin, G.-M.; Warden-Rothman, R.; Voigt, C. A. Retrosynthetic design of metabolic pathways to chemicals not found in nature. *Current Opinion in Systems Biology* **2019**, *14*, 82–107, ISBN: 2452-3100 Publisher: Elsevier.
- (2) Wu, S.; Snajdrova, R.; Moore, J. C.; Baldenius, K.; Bornscheuer, U. T. Biocatalysis: Enzymatic synthesis for industrial applications. *Angewandte Chemie International Edition* **2020**, ISBN: 1433-7851 Publisher: Wiley Online Library.
- (3) Arnold, F. H. Directed evolution: bringing new chemistry to life. *Angewandte Chemie International Edition* **2018**, *57*, 4143–4148.
- (4) Voigt, C. A. Synthetic biology 2020–2030: six commercially-available products that are changing our world. *Nature Communications* **2020**, *11*, 1–6, ISBN: 2041-1723 Publisher: Nature Publishing Group.
- (5) Huffman, M. A.; Fryszkowska, A.; Alvizo, O.; Borra-Garske, M.; Campos, K. R.; Devine, P. N.; Duan, D.; Forstater, J. H.; Grosser, S. T.; Halsey, H. M. Design of an in vitro biocatalytic cascade for the manufacture of islatravir. *Science* **2019**, *366*, 1255–1259, ISBN: 0036-8075 Publisher: American Association for the Advancement of Science.
- (6) Coley, C. W.; Green, W. H.; Jensen, K. F. Machine learning in computer-aided synthesis planning. *Accounts of chemical research* **2018**, *51*, 1281–1289, ISBN: 0001-4842 Publisher: ACS Publications.
- (7) Zheng, S.; Zeng, T.; Li, C.; Chen, B.; Coley, C. W.; Yang, Y.; Wu, R. BioNavi-NP: Biosynthesis Navigator for Natural Products. *arXiv preprint arXiv:2105.13121* **2021**,
- (8) Finnigan, W.; Hepworth, L. J.; Flitsch, S. L.; Turner, N. J. RetroBioCat as a computer-

- aided synthesis planning tool for biocatalytic reactions and cascades. *Nature Catalysis* **2021**, *4*, 98–104, ISBN: 2520-1158 Publisher: Nature Publishing Group.
- (9) Koch, M.; Duigou, T.; Faulon, J.-L. Reinforcement learning for bioretrosynthesis. *ACS synthetic biology* **2019**, *9*, 157–168, ISBN: 2161-5063 Publisher: ACS Publications.
- (10) Carbonell, P.; Wong, J.; Swainston, N.; Takano, E.; Turner, N. J.; Scrutton, N. S.; Kell, D. B.; Breitling, R.; Faulon, J.-L. Selenzyme: Enzyme selection tool for pathway design. *Bioinformatics* **2018**, *34*, 2153–2154.
- (11) Hult, K.; Berglund, P. Enzyme promiscuity: mechanism and applications. *Trends in biotechnology* **2007**, *25*, 231–238.
- (12) Bedbrook, C. N.; Yang, K. K.; Robinson, J. E.; Mackey, E. D.; Gradinaru, V.; Arnold, F. H. Machine learning-guided channelrhodopsin engineering enables minimally invasive optogenetics. *Nature methods* **2019**, 1–9, Publisher: Nature Publishing Group.
- (13) Wu, Z.; Kan, S. J.; Lewis, R. D.; Wittmann, B. J.; Arnold, F. H. Machine learning-assisted directed protein evolution with combinatorial libraries. *Proceedings of the National Academy of Sciences* **2019**, *116*, 8852–8858, Publisher: National Acad Sciences.
- (14) Fox, R. J.; Davis, S. C.; Mundorff, E. C.; Newman, L. M.; Gavrilovic, V.; Ma, S. K.; Chung, L. M.; Ching, C.; Tam, S.; Muley, S., et al. Improving catalytic function by ProSAR-driven enzyme evolution. *Nature biotechnology* **2007**, *25*, 338–344.
- (15) Bepler, T.; Berger, B. Learning protein sequence embeddings using information from structure. *arXiv preprint arXiv:1902.08661* **2019**,
- (16) Rao, R.; Bhattacharya, N.; Thomas, N.; Duan, Y.; Chen, P.; Canny, J.; Abbeel, P.; Song, Y. Evaluating protein transfer learning with TAPE. *Advances in Neural Information Processing Systems*. 2019; pp 9689–9701.

- (17) Rao, R. M.; Meier, J.; Sercu, T.; Ovchinnikov, S.; Rives, A. Transformer protein language models are unsupervised structure learners. *bioRxiv* **2020**, Publisher: Cold Spring Harbor Laboratory .eprint: <https://www.biorxiv.org/content/early/2020/12/15/2020.12.15.422761.full.pdf>.
- (18) Rives, A.; Meier, J.; Sercu, T.; Goyal, S.; Lin, Z.; Liu, J.; Guo, D.; Ott, M.; Zitnick, C. L.; Ma, J.; Fergus, R. Biological structure and function emerge from scaling unsupervised learning to 250 million protein sequences. *Proceedings of the National Academy of Sciences* **2021**, *118*, e2016239118.
- (19) Alley, E. C.; Khimulya, G.; Biswas, S.; AlQuraishi, M.; Church, G. M. Unified rational protein engineering with sequence-based deep representation learning. *Nature methods* **2019**, *16*, 1315–1322, Publisher: Nature Publishing Group.
- (20) Biswas, S.; Khimulya, G.; Alley, E. C.; Esvelt, K. M.; Church, G. M. Low-N protein engineering with data-efficient deep learning. *bioRxiv* **2020**, Publisher: Cold Spring Harbor Laboratory .eprint: <https://www.biorxiv.org/content/early/2020/01/24/2020.01.23.917682.full.pdf>.
- (21) Greenhalgh, J. C.; Fahlberg, S. A.; Pfleger, B. F.; Romero, P. A. Machine learning-guided acyl-ACP reductase engineering for improved in vivo fatty alcohol production. *bioRxiv* **2021**, Publisher: Cold Spring Harbor Laboratory.
- (22) Bonk, B. M.; Tarasova, Y.; Hicks, M. A.; Tidor, B.; Prather, K. L. Rational design of thiolase substrate specificity for metabolic engineering applications. *Biotechnology and bioengineering* **2018**, *115*, 2167–2182, ISBN: 0006-3592 Publisher: Wiley Online Library.
- (23) de Melo-Minardi, R. C.; Bastard, K.; Artiguenave, F. Identification of subfamily-specific sites based on active sites modeling and clustering. *Bioinformatics* **2010**, *26*, 3075–3082, ISBN: 1460-2059 Publisher: Oxford University Press.

- (24) Carbonell, P.; Wong, J.; Swainston, N.; Takano, E.; Turner, N. J.; Scrutton, N. S.; Kell, D. B.; Breitling, R.; Faulon, J.-L. Selenzyme: Enzyme selection tool for pathway design. *Bioinformatics* **2018**, *34*, 2153–2154, ISBN: 1367-4803 Publisher: Oxford University Press.
- (25) Rix, G.; Watkins-Dulaney, E. J.; Almhjell, P. J.; Boville, C. E.; Arnold, F. H.; Liu, C. C. Scalable continuous evolution for the generation of diverse enzyme variants encompassing promiscuous activities. *Nature Communications* **2020**, *11*, 5644, Number: 1 Publisher: Nature Publishing Group.
- (26) Chen, K.; Arnold, F. H. Enzyme Engineering for Nonaqueous Solvents: Random Mutagenesis to Enhance Activity of Subtilisin E in Polar Organic Media. *Bio/Technology* **1991**, *9*, 1073–1077, Number: 11 Publisher: Nature Publishing Group.
- (27) Romero, P. A.; Arnold, F. H. Exploring protein fitness landscapes by directed evolution. *Nature reviews Molecular cell biology* **2009**, *10*, 866–876, ISBN: 1471-0080 Publisher: Nature Publishing Group.
- (28) Chen, K.; Arnold, F. H. Engineering cytochrome P450s for enantioselective cyclopropanation of internal alkynes. *Journal of the American Chemical Society* **2020**, *142*, 6891–6895, ISBN: 0002-7863 Publisher: ACS Publications.
- (29) Corre, C.; Challis, G. L. New natural product biosynthetic chemistry discovered by genome mining. *Natural product reports* **2009**, *26*, 977–986, Publisher: Royal Society of Chemistry.
- (30) Colin, P.-Y.; Kintsjes, B.; Gielen, F.; Miton, C. M.; Fischer, G.; Mohamed, M. F.; Hyvönen, M.; Morgavi, D. P.; Janssen, D. B.; Hollfelder, F. Ultrahigh-throughput discovery of promiscuous enzymes by picodroplet functional metagenomics. *Nature communications* **2015**, *6*, 1–12, Publisher: Nature Publishing Group.

- (31) Fisher, B. F.; Snodgrass, H. M.; Jones, K. A.; Andorfer, M. C.; Lewis, J. C. Site-Selective C–H Halogenation Using Flavin-Dependent Halogenases Identified via Family-Wide Activity Profiling. *ACS central science* **2019**, *5*, 1844–1856, ISBN: 2374-7943 Publisher: ACS Publications.
- (32) Marshall, J. R.; Yao, P.; Montgomery, S. L.; Finnigan, J. D.; Thorpe, T. W.; Palmer, R. B.; Mangas-Sanchez, J.; Duncan, R. A. M.; Heath, R. S.; Graham, K. M.; Cook, D. J.; Charnock, S. J.; Turner, N. J. Screening and characterization of a diverse panel of metagenomic imine reductases for biocatalytic reductive amination. *Nature Chemistry* **2020**, 1–9, Publisher: Nature Publishing Group.
- (33) Kempa, E. E.; Galman, J. L.; Parmeggiani, F.; Marshall, J. R.; Malassis, J.; Fontenelle, C. Q.; Vendeville, J.-B.; Linclau, B.; Charnock, S. J.; Flitsch, S. L. Rapid Screening of Diverse Biotransformations for Enzyme Evolution. *Jacs Au* **2021**, *1*, 508–516, ISBN: 2691-3704 Publisher: ACS Publications.
- (34) Davis, M. I.; Hunt, J. P.; Herrgard, S.; Ciceri, P.; Wodicka, L. M.; Pallares, G.; Hocker, M.; Treiber, D. K.; Zarrinkar, P. P. Comprehensive analysis of kinase inhibitor selectivity. *Nature biotechnology* **2011**, *29*, 1046–1051, ISBN: 1546-1696 Publisher: Nature Publishing Group.
- (35) Schauer, N. J.; Magin, R. S.; Liu, X.; Doherty, L. M.; Buhrlage, S. J. Advances in discovering deubiquitinating enzyme (DUB) inhibitors. *Journal of medicinal chemistry* **2019**, *63*, 2731–2750, ISBN: 0022-2623 Publisher: ACS Publications.
- (36) Ernst, A. et al. A Strategy for Modulation of Enzymes in the Ubiquitin System. *Science* **2013**, *339*, 590–595, Publisher: American Association for the Advancement of Science Section: Report.
- (37) Hie, B.; Bryson, B. D.; Berger, B. Leveraging uncertainty in machine learning ac-

- celerates biological discovery and design. *Cell Systems* **2020**, *11*, 461–477. e9, ISBN: 2405-4712 Publisher: Elsevier.
- (38) Li, S.; Wan, F.; Shu, H.; Jiang, T.; Zhao, D.; Zeng, J. MONN: a multi-objective neural network for predicting compound-protein interactions and affinities. *Cell Systems* **2020**, *10*, 308–322. e11, ISBN: 2405-4712 Publisher: Elsevier.
- (39) Schomburg, I.; Chang, A.; Ebeling, C.; Gremse, M.; Heldt, C.; Huhn, G.; Schomburg, D. BRENDA, the enzyme database: updates and major new developments. *Nucleic acids research* **2004**, *32*, D431–D433, ISBN: 0305-1048 Publisher: Oxford University Press.
- (40) Fisher, B. F.; Snodgrass, H. M.; Jones, K. A.; Andorfer, M. C.; Lewis, J. C. Site-Selective C–H Halogenation Using Flavin-Dependent Halogenases Identified via Family-Wide Activity Profiling. *ACS Central Science* **2019**, *5*, 1844–1856, Publisher: American Chemical Society.
- (41) Yang, M.; Fehl, C.; Lees, K. V.; Lim, E.-K.; Offen, W. A.; Davies, G. J.; Bowles, D. J.; Davidson, M. G.; Roberts, S. J.; Davis, B. G. Functional and informatics analysis enables glycosyltransferase activity prediction. *Nature Chemical Biology* **2018**, *14*, 1109–1117, Number: 12 Publisher: Nature Publishing Group.
- (42) Robinson, S. L.; Smith, M. D.; Richman, J. E.; Aukema, K. G.; Wackett, L. P. Machine learning-based prediction of activity and substrate specificity for OleA enzymes in the thiolase superfamily. *Synthetic Biology* **2020**, *5*, Publisher: Oxford Academic.
- (43) Bastard, K. et al. Revealing the hidden functional diversity of an enzyme family. *Nature Chemical Biology* **2014**, *10*, 42–49, Number: 1 Publisher: Nature Publishing Group.
- (44) Martínez-Martínez, M. et al. Determinants and Prediction of Esterase Substrate Promiscuity Patterns. *ACS Chemical Biology* **2018**, *13*, 225–234, Publisher: American Chemical Society.

- (45) Huang, H. et al. Panoramic view of a superfamily of phosphatases through substrate profiling. *Proceedings of the National Academy of Sciences* **2015**, *112*, E1974–E1983, Publisher: National Academy of Sciences Section: PNAS Plus.
- (46) Kim, P.; Winter, R.; Clevert, D.-A. Deep Protein-Ligand Binding Prediction Using Unsupervised Learned Representations. *ChemRxiv* **2020**,
- (47) Jin, W.; Barzilay, R.; Jaakkola, T. Junction tree variational autoencoder for molecular graph generation. International Conference on Machine Learning. 2018; pp 2323–2332.
- (48) Morgan, H. L. The generation of a unique machine description for chemical structures—a technique developed at chemical abstracts service. *Journal of Chemical Documentation* **1965**, *5*, 107–113, ISBN: 0021-9576 Publisher: ACS Publications.
- (49) Pettersen, E. F.; Goddard, T. D.; Huang, C. C.; Couch, G. S.; Greenblatt, D. M.; Meng, E. C.; Ferrin, T. E. UCSF Chimera—a visualization system for exploratory research and analysis. *Journal of computational chemistry* **2004**, *25*, 1605–1612.
- (50) Jumper, J.; Evans, R.; Pritzel, A.; Green, T.; Figurnov, M.; Tunyasuvunakool, K.; Ronneberger, O.; Bates, R.; Zidek, A.; Bridgland, A. High accuracy protein structure prediction using deep learning. *Fourteenth Critical Assessment of Techniques for Protein Structure Prediction (Abstract Book)* **2020**, *22*, 24.
- (51) Jumper, J.; Evans, R.; Pritzel, A.; Green, T.; Figurnov, M.; Ronneberger, O.; Tunyasuvunakool, K.; Bates, R.; Židek, A.; Potapenko, A., et al. Highly accurate protein structure prediction with AlphaFold. *Nature* **2021**, 1–11.
- (52) Baek, M.; DiMaio, F.; Anishchenko, I.; Dauparas, J.; Ovchinnikov, S.; Lee, G. R.; Wang, J.; Cong, Q.; Kinch, L. N.; Schaeffer, R. D., et al. Accurate prediction of protein structures and interactions using a three-track neural network. *Science* **2021**,

- (53) Akiba, T.; Sano, S.; Yanase, T.; Ohta, T.; Koyama, M. Optuna: A next-generation hyperparameter optimization framework. Proceedings of the 25th ACM SIGKDD international conference on knowledge discovery & data mining. 2019; pp 2623–2631.
- (54) Paszke, A.; Gross, S.; Massa, F.; Lerer, A.; Bradbury, J.; Chanan, G.; Killeen, T.; Lin, Z.; Gimelshein, N.; Antiga, L. Pytorch: An imperative style, high-performance deep learning library. *arXiv preprint arXiv:1912.01703* **2019**,
- (55) Pedregosa, F.; Varoquaux, G.; Gramfort, A.; Michel, V.; Thirion, B.; Grisel, O.; Blondel, M.; Prettenhofer, P.; Weiss, R.; Dubourg, V. Scikit-learn: Machine learning in Python. *the Journal of machine Learning research* **2011**, *12*, 2825–2830, ISBN: 1532-4435 Publisher: JMLR. org.
- (56) Chollet, F., et al. Keras. <https://keras.io>, 2015.
- (57) Cock, P. J.; Antao, T.; Chang, J. T.; Chapman, B. A.; Cox, C. J.; Dalke, A.; Friedberg, I.; Hamelryck, T.; Kauff, F.; Wilczynski, B. Biopython: freely available Python tools for computational molecular biology and bioinformatics. *Bioinformatics* **2009**, *25*, 1422–1423, ISBN: 1460-2059 Publisher: Oxford University Press.
- (58) Swain, M. CIRpy-A Python interface for the Chemical Identifier Resolver (CIR). *Matt Swain's Blog* **2012**,
- (59) Kim, S.; Thiessen, P. A.; Bolton, E. E.; Chen, J.; Fu, G.; Gindulyte, A.; Han, L.; He, J.; He, S.; Shoemaker, B. A. PubChem substance and compound databases. *Nucleic acids research* **2016**, *44*, D1202–D1213, ISBN: 1362-4962 Publisher: Oxford University Press.
- (60) Consortium, U. UniProt: a hub for protein information. *Nucleic acids research* **2015**, *43*, D204–D212, ISBN: 1362-4962 Publisher: Oxford University Press.
- (61) Bateman, A.; Coin, L.; Durbin, R.; Finn, R. D.; Hollich, V.; Griffiths-Jones, S.; Khanna, A.; Marshall, M.; Moxon, S.; Sonnhammer, E. L. The Pfam protein families

database. *Nucleic acids research* **2004**, *32*, D138–D141, ISBN: 0305-1048 Publisher: Oxford University Press.

- (62) Finn, R. D.; Clements, J.; Eddy, S. R. HMMER web server: interactive sequence similarity searching. *Nucleic acids research* **2011**, *39*, W29–W37, ISBN: 0305-1048 Publisher: Oxford University Press.

Supporting Information

Machine learning modeling of family wide enzyme-substrate specificity screens

Samuel Goldman,^{†,⊥} Ria Das,^{¶,⊥} Kevin K. Yang,[§] and Connor W. Coley^{⊥,¶,*}

[†]*MIT Computational and Systems Biology*

[¶]*MIT Electrical Engineering and Computer Science*

[§]*Microsoft Research New England*

[⊥]*MIT Chemical Engineering*

*E-mail: ccoley@mit.edu

Data

Halogenase data

Halogenase data was prepared as described by Fisher et al. They measure the activity of 87 different proteins against 62 substrates using high throughput LC-MS based screening.⁴⁰ However, many sampled enzymes are either insoluble or display no halogenation activity. We subset the proteins to a smaller set of 42 proteins that have some halogenation activity on at least one of the substrates tested. We binarize data at the 8% conversion threshold, which Fisher et al. report as removing false positives. Further, rather than test activity on both the chlorination and bromination activity labels, we opt to use only the dataset measuring bromination, which has more a higher percentage of active conversions.

SMILES strings are extracted from the ChemDraw file provided by Fisher et al. All protein sequences with greater than 1000 amino acids were filtered from the enzyme dataset.

Phosphatase data

Phosphatase data is extracted from SI tables provided by Huang et al. Compounds listed in the results using common names are converted using a combination of PubChem’s name converter, cirpy, and manual re-drawing according to compounds in the SI.^{58,59}

Sequence IDs are mapped to amino acid sequences using the UniProt database. All entries that are no longer valid are identified using the UniParc database.⁶⁰ Enzyme-substrate hits are called at a binary threshold cutoff of 0.2 OD as described in the original paper to correct for background noise.

BKACE data

β-ketoacid cleavage enzyme (BKACE) substrates are manually re-drawn and SMILES strings are extracted from ChemDraw.⁴³ Enzyme sequences are extracted from the SI, and all hits are binarized according to original procedure from Bastard et al. using a mixture of Gaussians.

Thiolase data

Binary thiolase data is used and extracted as prepared by Robinson et al. and binarized at a threshold of 1×10^{-8} .⁴²

Esterase data

Binary esterase data is used and extracted as prepared by Martínez-Martínez et al. All enzymes that display > 0 activity are considered to be hits after binarization.⁴⁴

Glycosyltransferase data

Glycosyltransferase acceptors and donors were originally measured and classified as having no, intermediate, or strong activity using a “green”, “amber”, or “red” classification system.⁴¹ We make the simplifying assumption to treat all intermediate activity enzymes as a positive example in our binary classification formulation. Further, many more glycosyltransferase acceptor substrates are tested than donors, and so we choose to predict activity of glycosyltransferase-glycosyl acceptor substrate pairs. We use ChemDraw to extract acceptor substrate SMILES strings.

Kinase data

The kinase data in this study is a panel of inhibitors screened against kinases, originally collected by Davis et al.³⁴ To compare models directly to Hie et al., we use identical data preprocessing and featurization.³⁷

For the analysis of structure based pooling, we further processed this dataset for consistency with family-wide protein screens. We subset the data to represent a single PFAM family, PF00069,⁶¹ and we use the `hmmsearch` tool to identify all proteins that satisfy this domain.⁶²

Due to the large size of the kinase proteins, individual kinase domains were experimentally cloned separately. Some protein entries have multiple measurements corresponding to the first and second kinase domains within the protein. To account for this, we use the envelope returned from `hmmsearch` to subset each protein down to its relevant domain(s). In the interest of maintaining a dataset without point mutations, we further remove all proteins that have specific deletions or insertions. Finally, all kinase-inhibitors without a measured K_d are given a default value of 10,000 as set by Hie et al.

Table S1: Active site structure references used in pooling. All structure informed pooling strategies require a catalytic center in order to define various angstrom shells of residues to pool over. This table provides the PDB reference crystal structure as well as the reference residues or structural elements used to define the pooling center, from which spherical radii originate.

Dataset	PDB Ref.	Ref. type	Ref.
Halogenase ⁴⁰	2AR8	ligand	7-chlorotryptophan
Glycosyltransferase ⁴¹	3HBF	ligands	UDP and 3,5,7-TRIHYDROXY-2-(3,4,5-TRIHYDROXYPHENYL)-4H-CHROMEN-4-ONE
Thiolase ⁴²	4KU5	catalytic residue	C143
BKACE ⁴³	2Y7F	ligand	(5S)-5-amino-3-oxo-hexanoic-acid
Phosphatase ⁴⁵	3L8E	ligand	acetic acid
Esterase ⁴⁴	5A6V	catatlytic residues	S105, D187D, H224
Kinase (inhibitors) ³⁴	2CN5	ligand	ADP

Table S2: Summary of valid substrate and sequence “tasks”. In each dataset, only certain substrates and sequences are defined as valid “tasks” based upon the balance between active and inactive examples. Each substrate or sequence used for an enzyme or substrate discovery task respectively requires at least 2 positive examples and at a minimum, 10% of examples in that task must be part of the minority class. This table defines the number of valid substrate and sequence tasks.

Dataset	Num entries	# Seqs.	# Subs.	Valid subs.	Valid seqs.
Thiolase	1095	73	15	11	70
Halogenase	2604	42	62	20	17
BKACE	2737	161	17	7	54
Glyco.	4347	54	91	35	48
Esterase	14016	146	96	59	106
Phosphatase	35970	218	165	103	102

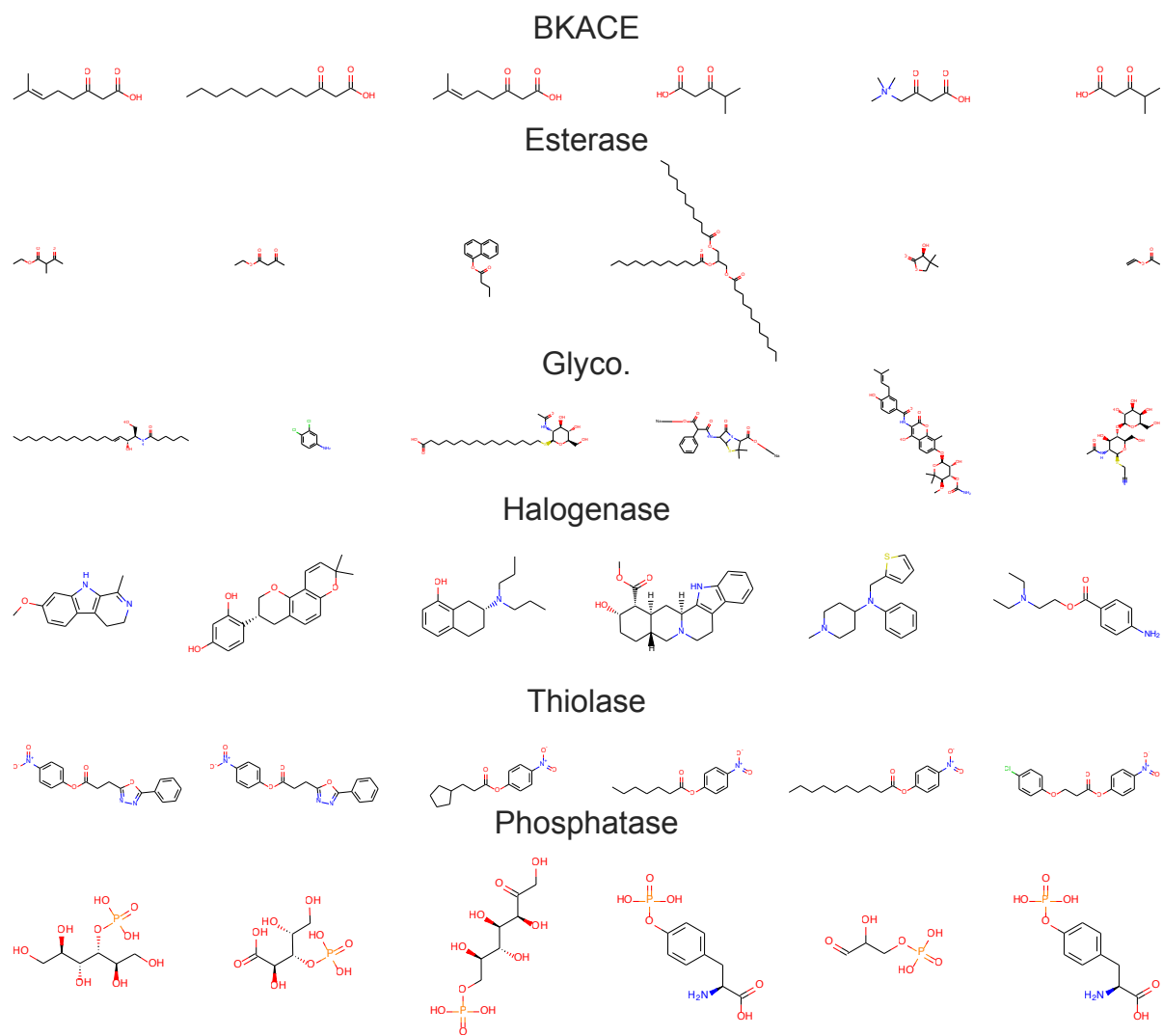


Figure S1: **Dataset substrates** 6 exemplar molecule substrates are randomly chosen from each dataset and displayed.

Enzyme and Substrate Dataset Diversity

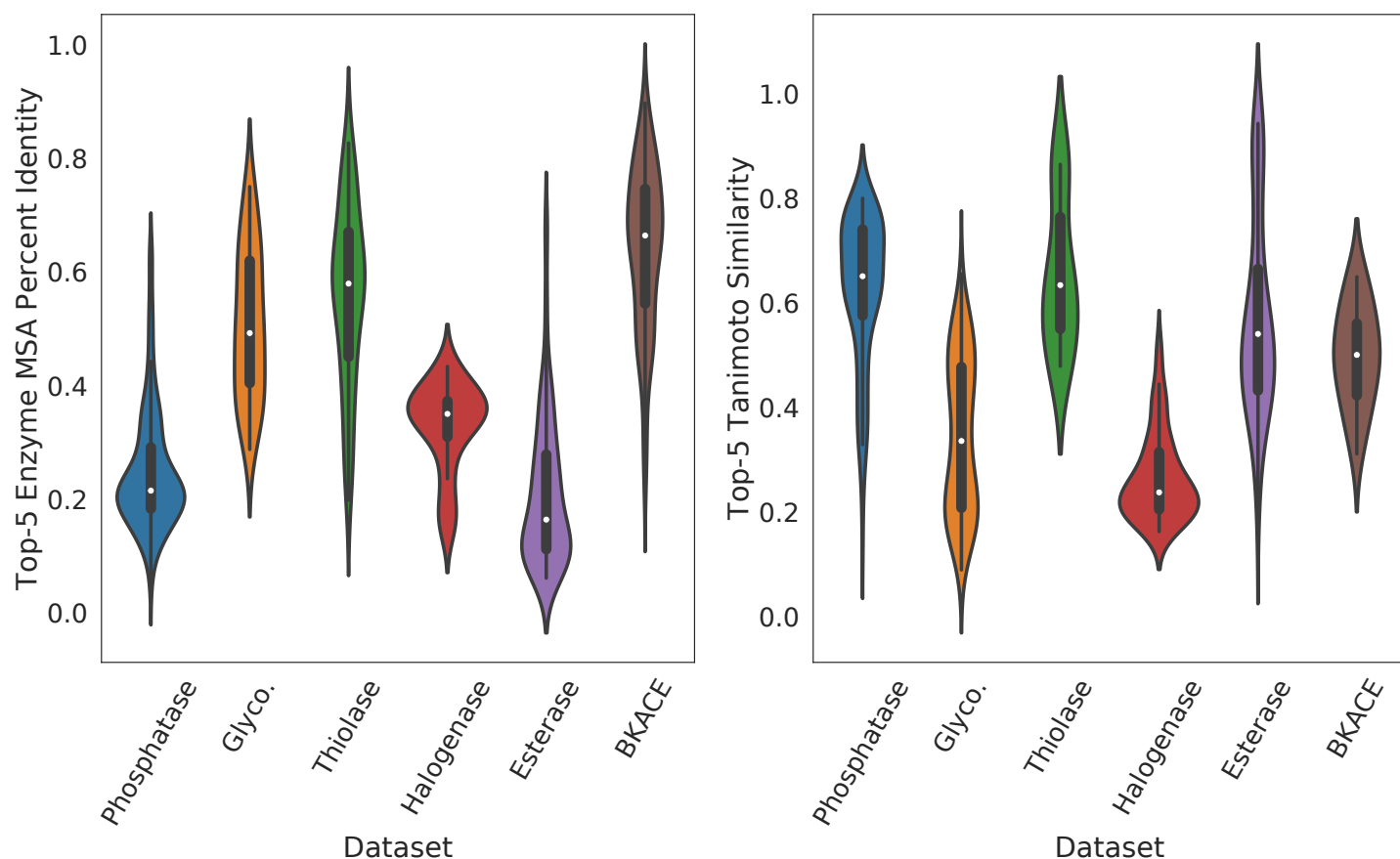


Figure S2: **Dataset diversity** Distributions of top-5 enzyme similarity (left) and substrate similarity (right) are shown across enzyme datasets collected. Enzyme similarity is calculated as the percent overlap between two sequences in their respective multiple sequence alignment, excluding positions where both sequences contain gaps. Substrate similarity is computed using Tanimoto similarity between 2048-bit chiral Morgan fingerprints.

Extended results

Table S3: Full enzyme discovery area under the precision recall curve (AUPRC) results. On the 5 different datasets tested, K-nearest neighbor baselines with Levenshtein edit distance are compared against feed-forward networks using various featurizations and ridge regression models. Pretrained features (“ESM-1b”) indicate protein features extracted from a masked language model trained on UniRef50.¹⁸ Two compound protein interaction architectures are tested, both concatenation and dot products, indicated with “[{prot repr.}, {sub repr.}]” and “[prot repr.]•[sub repr.]” respectively. Halogenase and glycosyltransferase datasets are evaluated using leave-one-out splits, whereas BKACE, phosphatase, and esterase datasets are evaluated with 5 repeats of 10 different cross validation splits. Average precision is calculated using scikit-learn for each substrate task separately before being averaged. Average values are presented across 3 random seeds \pm standard error

Method Type	Dataset Method	BKACE	Esterase	Glyco.	Halogenase	Phosphatase
Baselines	KNN: Levenshtein	0.564 \pm 0.011	0.528 \pm 0.002	0.539 \pm 0.003	0.375 \pm 0.014	0.316 \pm 0.004
CPI	FFN: [ESM-1b, Morgan]	0.478 \pm 0.012	0.579 \pm 0.007	0.581 \pm 0.008	0.489 \pm 0.025	0.386 \pm 0.006
	FFN: ESM-1b • Morgan	0.645 \pm 0.007	0.588 \pm 0.011	0.559 \pm 0.010	0.463 \pm 0.021	0.389 \pm 0.002
Multi-task	FFN: [ESM-1b, one-hot]	0.433 \pm 0.007	0.557 \pm 0.007	0.526 \pm 0.024	0.510 \pm 0.043	0.361 \pm 0.008
	FFN: ESM-1b	0.664 \pm 0.011	0.572 \pm 0.008	0.543 \pm 0.024	0.420 \pm 0.003	0.359 \pm 0.005
Single-task	Ridge: ESM-1b	0.648 \pm 0.011	0.583 \pm 0.003	0.575 \pm 0.000	0.446 \pm 0.000	0.413 \pm 0.005

Table S4: Full enzyme discovery area under the receiver operating curve (AUC-ROC) results. On the 5 different datasets tested, K-nearest neighbor baselines with Levenshtein edit distance are compared against feed-forward networks using various featurizations and ridge regression models. ESM-1b features indicate protein features extracted from a masked language model trained on UniRef50 .¹⁸ Two compound protein interaction architectures are tested, both concatenation and dot products, indicated with “[{prot repr.}, {sub repr.}]” and “[{prot repr.}•{sub repr.}]” respectively. Halogenase and glycosyltransferase datasets are evaluated using leave-one-out splits, whereas BKACE, phosphatase, and esterase datasets are evaluated with 5 repeats of 10 different cross validation splits. AUC ROC is calculated using scikit-learn for each substrate task separately before being averaged. Average values are presented across 3 random seeds \pm standard error

Method Type	Dataset Method	BKACE	Esterase	Glyco.	Halogenase	Phosphatase
Baselines	KNN: Levenshtein	0.896 \pm 0.003	0.686 \pm 0.002	0.623 \pm 0.002	0.506 \pm 0.013	0.635 \pm 0.003
CPI	FFN: [ESM-1b, Morgan]	0.793 \pm 0.001	0.723 \pm 0.003	0.636 \pm 0.019	0.568 \pm 0.036	0.676 \pm 0.008
	FFN: ESM-1b • Morgan	0.884 \pm 0.002	0.730 \pm 0.004	0.647 \pm 0.021	0.587 \pm 0.025	0.678 \pm 0.001
Multi-task	FFN: [ESM-1b, one-hot]	0.768 \pm 0.006	0.714 \pm 0.006	0.586 \pm 0.018	0.616 \pm 0.043	0.657 \pm 0.002
	FFN: ESM-1b	0.892 \pm 0.002	0.713 \pm 0.002	0.624 \pm 0.025	0.564 \pm 0.003	0.669 \pm 0.004
Single-task	Ridge: ESM-1b	0.892 \pm 0.004	0.725 \pm 0.001	0.653 \pm 0.000	0.567 \pm 0.000	0.703 \pm 0.002

Table S5: Full substrate discovery area under the precision recall curve (AUPRC) results. CPI models and single task models are compared on the glycosyltransferase, esterase, and phosphatase datasets, all with 5 trials of 10-fold cross validation. Each model and featurization is compared to “Ridge: Morgan” using a 2-sided Welch T test, with each additional asterisk representing significance at [0.05, 0.01, 0.001, 0.0001] thresholds respectively after applying a Benjamini-Hochberg correction. Pretrained substrate featurizations used in “Ridge: pretrained” are features extracted from a junction-tree variational auto-encoder (JT-VAE).⁴⁷ Two compound protein interaction architectures are tested, both concatenation and dot-product, indicated with “[{prot repr.}, {sub repr.}]” and “[{prot repr.}•{sub repr.}]” respectively. In the interaction based architectures, ESM-1b indicates the use of a masked language model trained on UniRef50 as a protein representation .¹⁸ Average precision is calculated using scikit-learn for each substrate task separately before being averaged. Models are hyperparameter optimized on a held out halogenase dataset. Values represent mean values across 3 random seeds \pm standard error

Method Type	Dataset Method	Esterase	Glyco.	Phosphatase
Baselines	KNN: Tanimoto	0.609 \pm 0.008	0.588 \pm 0.006	0.426 \pm 0.002
	Ridge: random feats.	0.327 \pm 0.014	0.239 \pm 0.032	0.294 \pm 0.006
CPI	FFN: [ESM-1b, Morgan]	0.674 \pm 0.019	0.673 \pm 0.010	0.462 \pm 0.006
	FFN: ESM-1b • Morgan	0.709 \pm 0.018	0.693 \pm 0.005	0.506 \pm 0.004
Multi-task	FFN: Morgan	0.654 \pm 0.011	0.689 \pm 0.005	0.442 \pm 0.001
	FFN: [one-hot, Morgan]	0.707 \pm 0.019	0.677 \pm 0.009	0.493 \pm 0.005
Single-task	Ridge: Morgan	0.716 \pm 0.010	0.699 \pm 0.008	0.504 \pm 0.002
	Ridge: pretrained	0.489 \pm 0.004	0.505 \pm 0.007	0.411 \pm 0.002

Table S6: Full substrate discovery area under the receiver operating curve (AUC-ROC) results. CPI models and single task models are compared on the glycosyltransferase, esterase, and phosphatase datasets, all with 5 trials of 10-fold cross validation. Each model and featurization is compared to “Ridge: Morgan” using a 2-sided Welch T test, with each additional asterisk representing significance at [0.05, 0.01, 0.001, 0.0001] thresholds respectively after applying a Benjamini-Hochberg correction. Pretrained substrate featurizations used in “Ridge: pretrained” are features extracted from a junction-tree variational auto-encoder (JT-VAE).⁴⁷ Two compound protein interaction architectures are tested, both concatenation and dot-product, indicated with “[{prot repr.}, {sub repr.}]]” and “[{prot repr.}•{sub repr.}]” respectively. In the interaction based architectures, “ESM-1b” indicates the use of a masked language model trained on UniRef50 as a protein representation.¹⁸ Models are hyperparameter optimized on a held out halogenase dataset. Values represent mean values across 3 random seeds \pm standard error

Method Type	Dataset Method	Esterase	Glyco.	Phosphatase
Baselines	KNN: Tanimoto	0.807 ± 0.001	0.855 ± 0.004	0.680 ± 0.002
	Ridge: random feats.	0.513 ± 0.019	0.483 ± 0.042	0.481 ± 0.011
CPI	FFN: [ESM-1b, Morgan]	0.808 ± 0.005	0.883 ± 0.004	0.689 ± 0.004
	FFN: ESM-1b • Morgan	0.831 ± 0.003	0.892 ± 0.001	0.715 ± 0.003
Multi-task	FFN: Morgan	0.784 ± 0.004	0.880 ± 0.007	0.675 ± 0.002
	FFN: [one-hot, Morgan]	0.833 ± 0.006	0.880 ± 0.002	0.711 ± 0.005
Single-task	Ridge: Morgan	0.841 ± 0.003	0.878 ± 0.005	0.710 ± 0.001
	Ridge: pretrained	0.724 ± 0.003	0.751 ± 0.004	0.641 ± 0.001

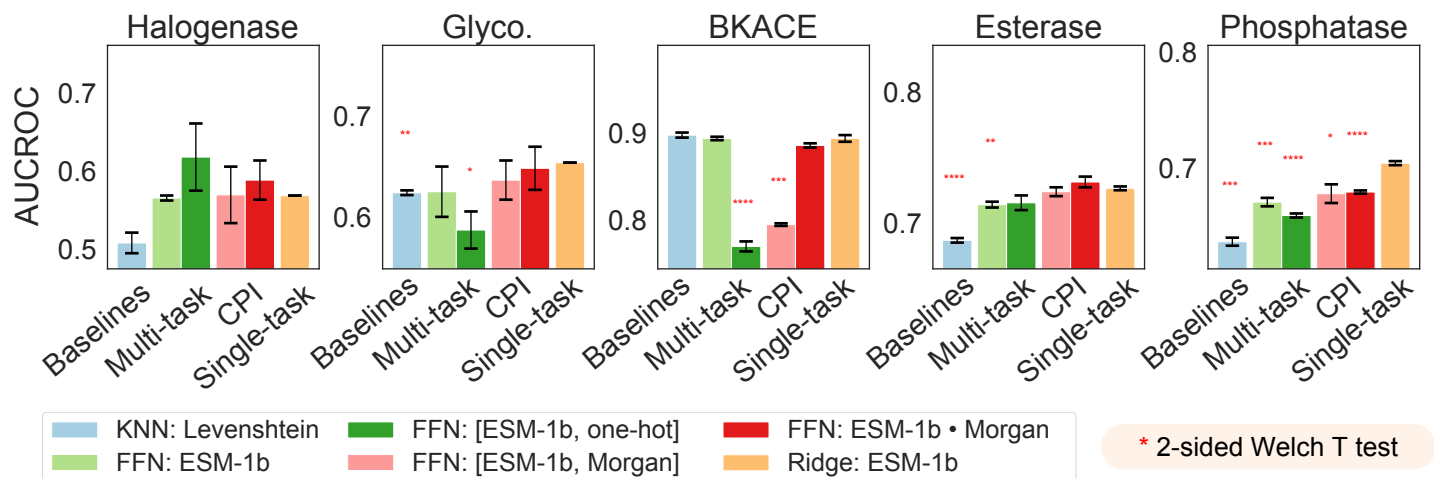


Figure S3: **Enzyme discovery benchmarking with AUCROC** On the 5 different datasets tested, K-nearest neighbor baselines with Levenshtein edit distance are compared against feed-forward networks using various featurizations and ridge regression models in terms of AUC ROC performance. ESM-1b features indicate protein features extracted from a masked language model trained on UniRef50.¹⁸ Concatenation and dot product architectures are indicated with “[{prot repr.}, {sub repr.}]” and “[{prot repr.}•{sub repr.}]” respectively. Halogenase and glycosyltransferase datasets are evaluated using leave-one-out splits. BKACE, phosphatase, and esterase datasets are evaluated with 5 repeats of 10 different cross validation splits. AUC ROC is calculated using scikit-learn for each substrate task separately before being averaged. Error bars represent the standard error of the mean across 3 random seeds. Each model and featurization is compared to “Ridge: ESM-1b” using a 2-sided Welch T test, with each additional asterisk representing significance at [0.05, 0.01, 0.001, 0.0001] thresholds respectively after applying a Benjamini-Hochberg correction.

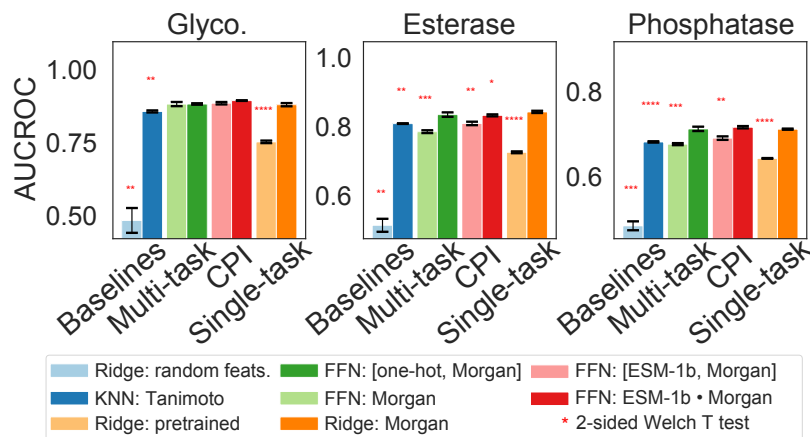


Figure S4: **Full substrate discovery AUC ROC results.** CPI models and single task models are compared on the glycosyltransferase, esterase, and phosphatase datasets, all with 5 trials of 10-fold cross validation. Error bars represent the standard error of the mean across 3 random seeds. Each model and featurization is compared to “Ridge: Morgan” using a 2-sided Welch T test, with each additional asterisk representing significance at [0.05, 0.01, 0.001, 0.0001] thresholds respectively after applying a Benjamini-Hochberg correction. Pretrained substrate featurizations used in “Ridge: pretrained” are features extracted from a junction-tree variational auto-encoder (JT-VAE).⁴⁷ Concatenation and dot-product architectures are indicated with “[{prot repr.}, {sub repr.}]” and “[{prot repr.}•{sub repr.}]” respectively. In the interaction based architectures, “ESM-1b” indicates the use of a masked language model trained on UniRef50 as a protein representation.¹⁸ Models are hyperparameter optimized on a held out halogenase dataset.

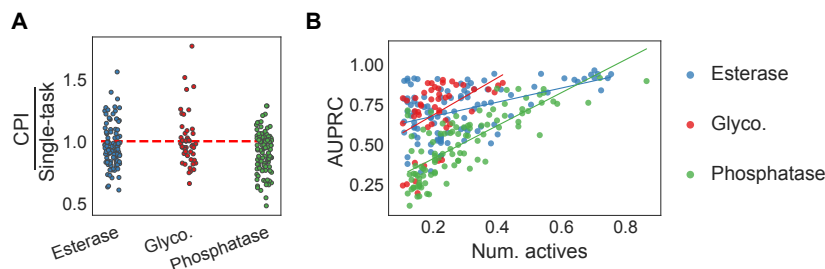


Figure S5: **Substrate Discovery Extended Analysis (A)** Average AUPRC on each individual “enzyme task” is compared between compound protein interaction models and single-task models. Points below 1 indicate substrates on which single-task models better predict enzyme activity than CPI models. CPI models used are “FFN: [ESM-1b, Morgan]” and single-task models are “Ridge: Morgan”. **(B)** AUPRC values from the ridge regression model broken out by each task are plotted against the fraction of active enzymes in the dataset. Best fit lines are drawn through each dataset to serve as a visual guide.

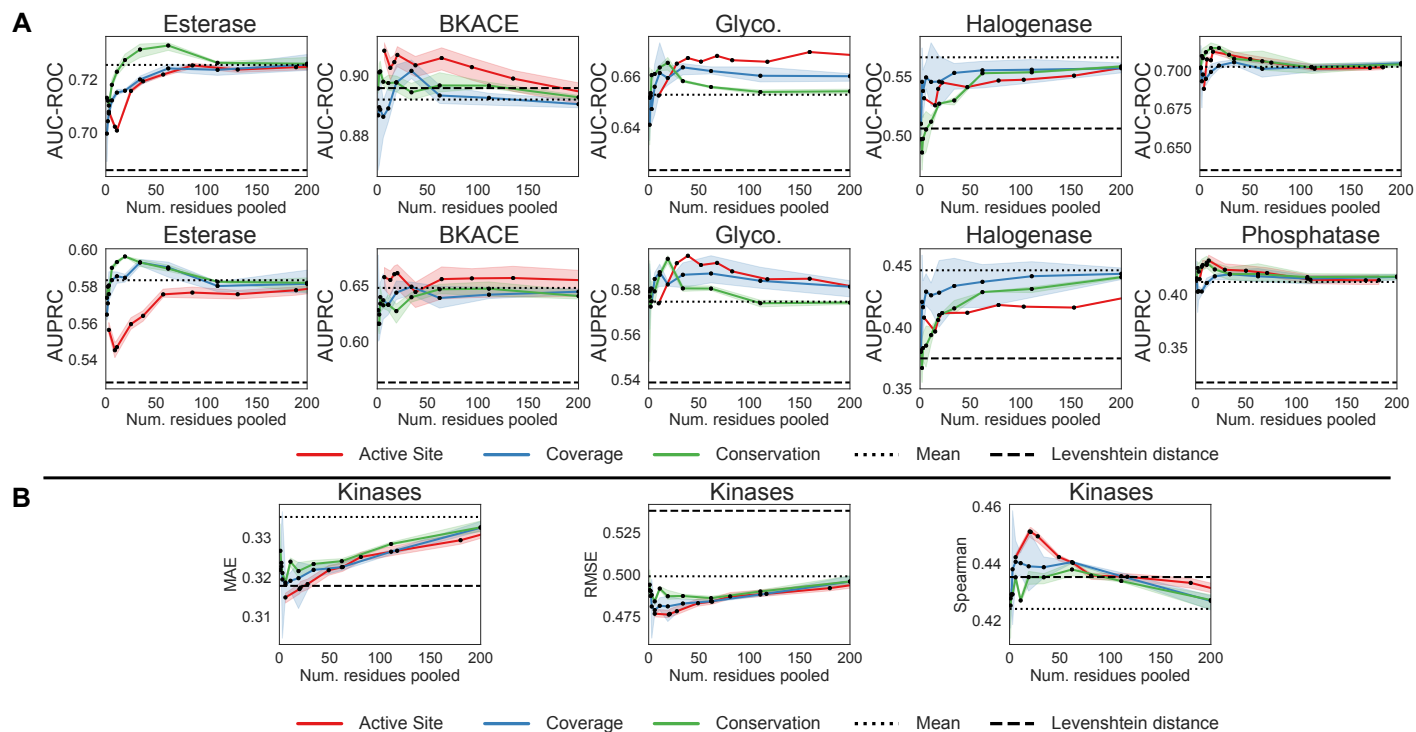


Figure S6: **MSA and structure based pooling across all datasets tested** (A) Active site, coverage, conservation, and mean pooling are plotted for all 5 enzyme discovery datasets tested. Both AUCROC and AUPRC values are shown. These are compared against the Levenshtein distance baseline (dotted). (B) Equivalent analysis is conducted on the filtered kinase dataset extracted from Davis et al. with MAE, RMSE, and Spearman rank correlation shown.³⁴ The same hyperparameters are used as set in Figure 2 for ridge regression models. All experiments are repeated for 3 random seeds following the same split evaluation as in other enzyme discovery model benchmarking.

Prediction outputs

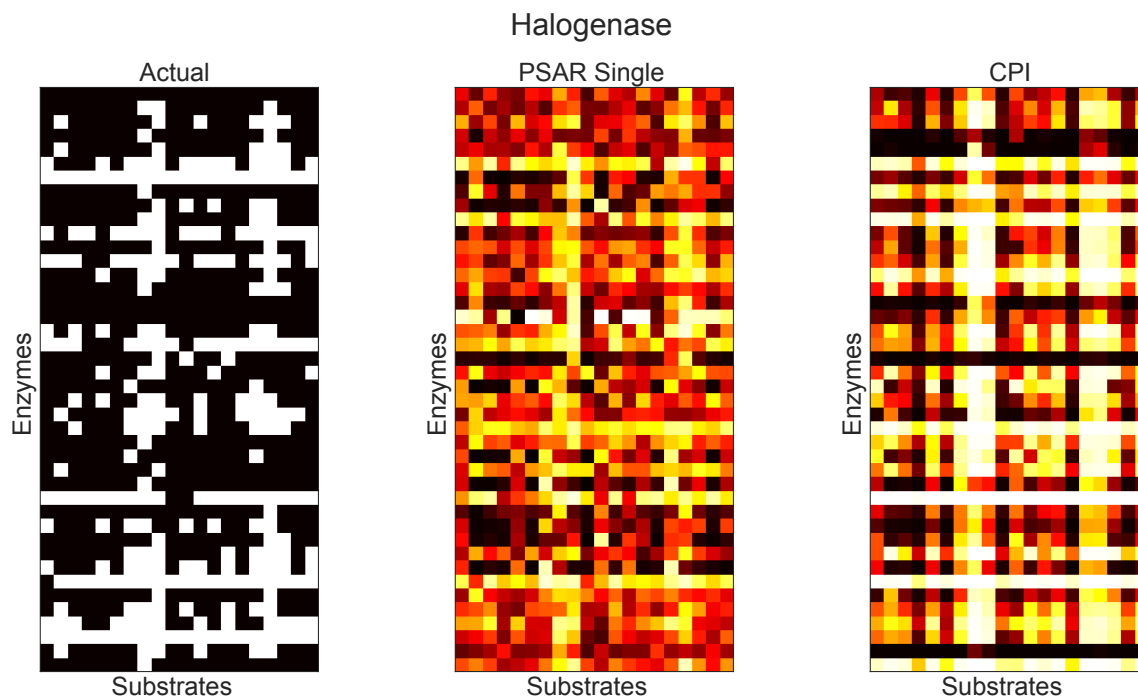


Figure S7: **Enzyme discovery halogenase prediction results** Ground truth binary enzyme-substrate activities (left) are compared against a single seed of predictions made through cross validation using a single-task ridge regression model (middle) and a CPI based model, FFN: [ESM-1b, Morgan] (right).

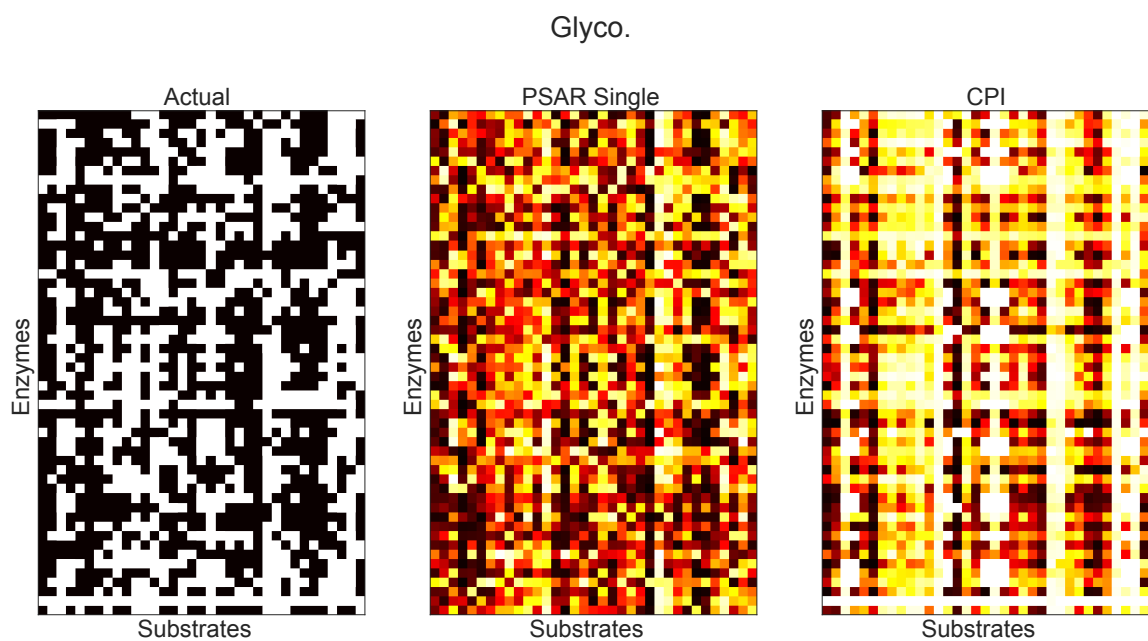


Figure S8: **Enzyme discovery glycosyltransferase prediction results** Ground truth binary enzyme-substrate activities (left) are compared against a single seed of predictions made through cross validation using a single-task ridge regression model (middle) and a CPI based model, FFN: [ESM-1b, Morgan] (right).

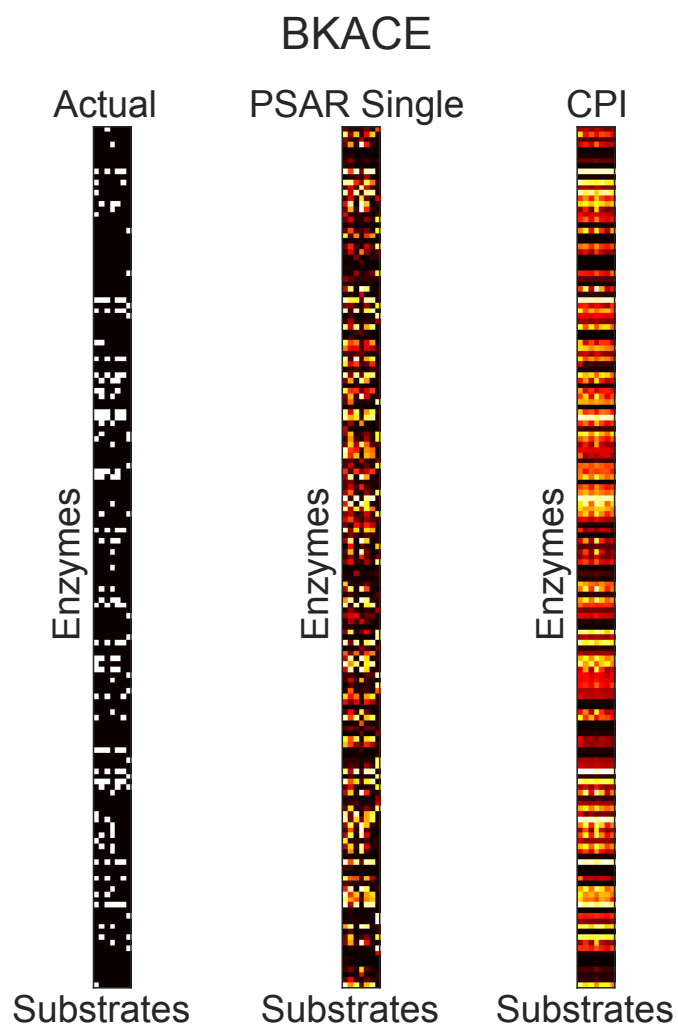


Figure S9: **Enzyme discovery BKACE prediction results** Ground truth binary enzyme-substrate activities (left) are compared against a single seed of predictions made through cross validation using a single-task ridge regression model (middle) and a CPI based model, FFN: [ESM-1b, Morgan] (right).

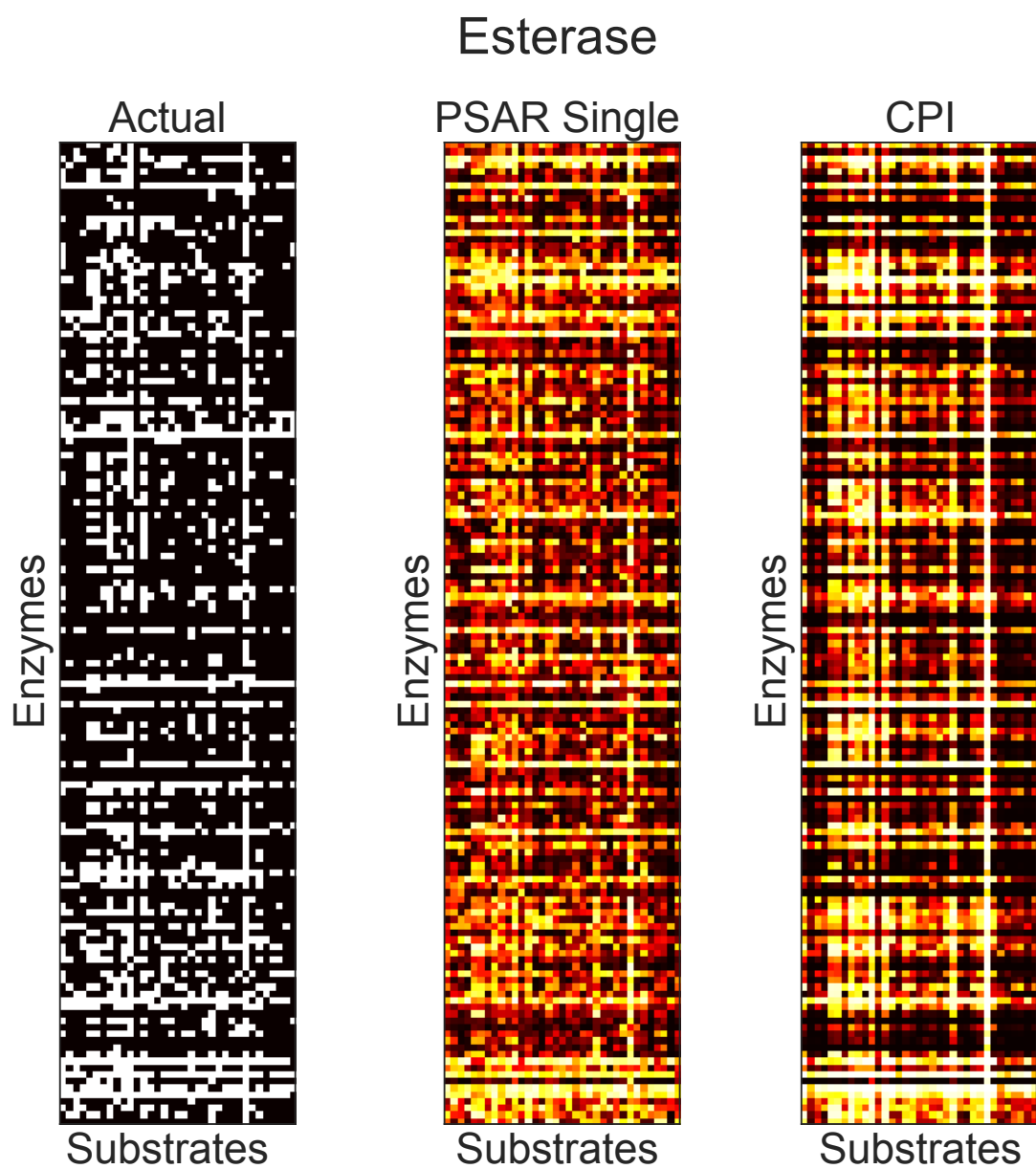


Figure S10: **Enzyme discovery esterase prediction results** Ground truth binary enzyme-substrate activities (left) are compared against a single seed of predictions made through cross validation using a single-task ridge regression model (middle) and a CPI based model, FFN: [ESM-1b, Morgan] (right).

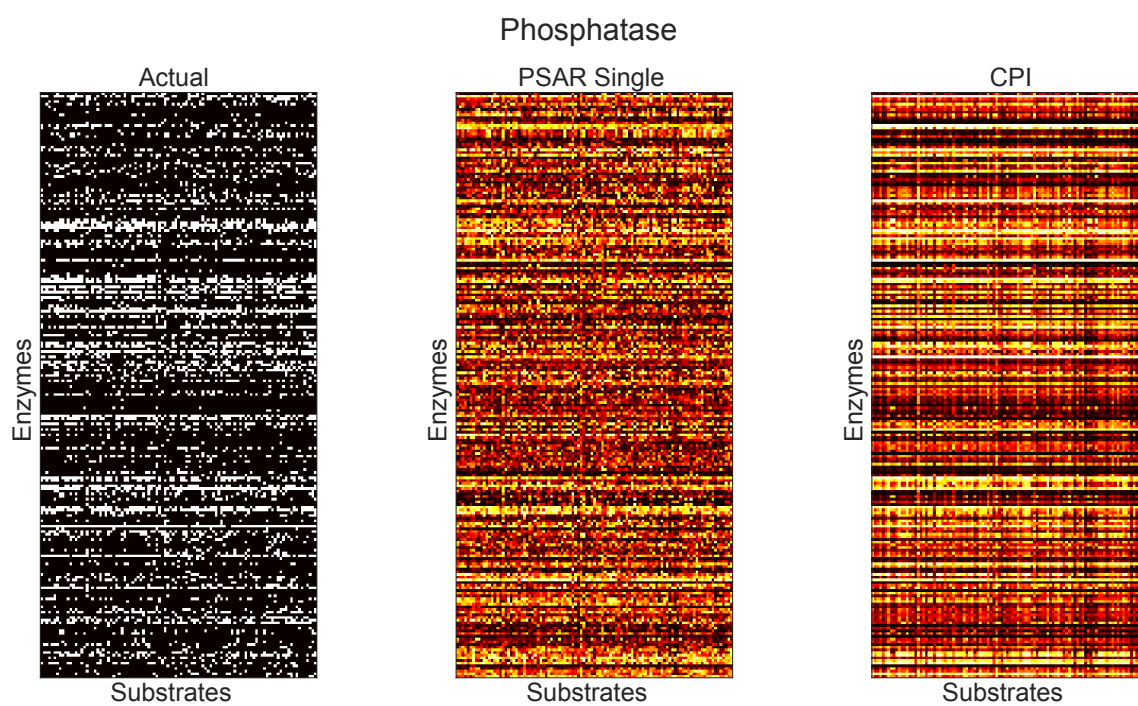


Figure S11: **Enzyme discovery phosphatase prediction results** Ground truth binary enzyme-substrate activities (left) are compared against a single seed of predictions made through cross validation using a single-task ridge regression model (middle) and a CPI based model, FFN: [ESM-1b, Morgan] (right).

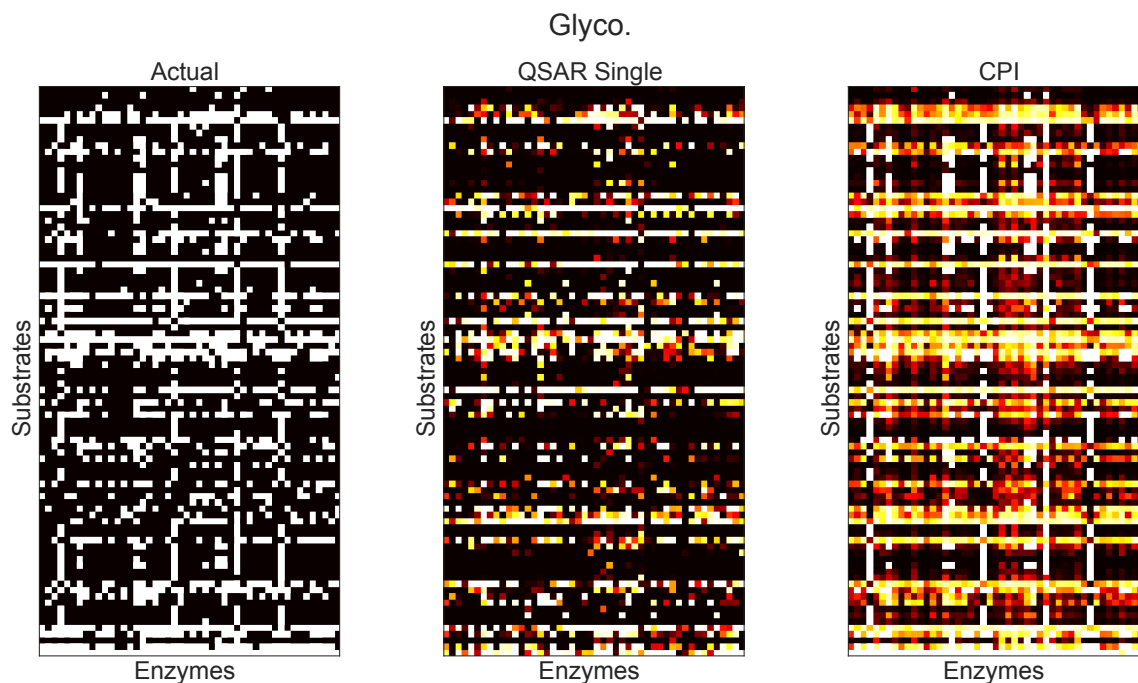


Figure S12: **Substrate discovery glycosyltransferase prediction results** Ground truth binary enzyme-substrate activities (left) are compared against a single seed of predictions made through cross validation using a single-task ridge regression model (middle) and a CPI based model, FFN: [ESM-1b, Morgan] (right).

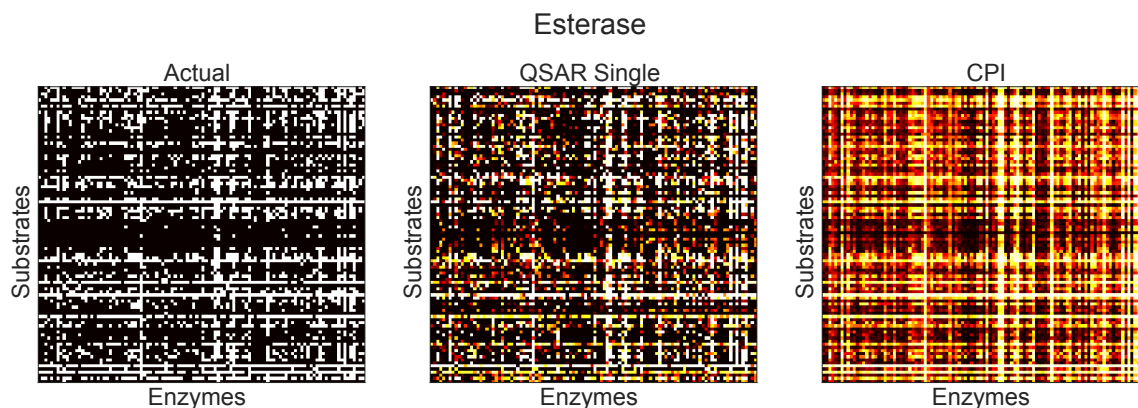


Figure S13: **Substrate discovery esterase prediction results** Ground truth binary enzyme-substrate activities (left) are compared against a single seed of predictions made through cross validation using a single-task ridge regression model (middle) and a CPI based model, FFN: [ESM-1b, Morgan] (right).

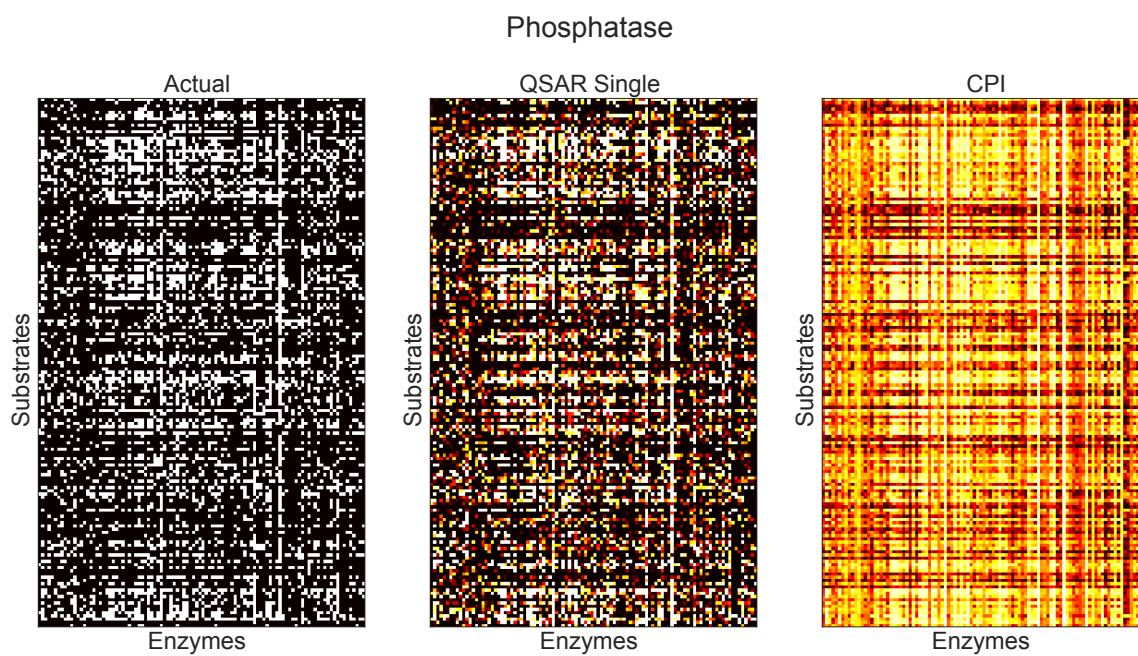


Figure S14: **Substrate discovery phosphatase prediction results** Ground truth binary enzyme-substrate activities (left) are compared against a single seed of predictions made through cross validation using a single-task ridge regression model (middle) and a CPI based model, FFN: [ESM-1b, Morgan] (right).